APPENDIX A. THE ACCURACY OF THE CALCULATED PROFILES

A.1 Relative Accuracies With Smooth Virtual Height Curves

The analysis of a finite number of exact virtual-height data points does not, in general, give exact real heights. Errors are introduced primarily through the inability of the analysis procedure to reproduce exactly the true variation of plasma frequency with height between the scaled frequencies. For the simplest method of analysis using linear laminations (Mode 1 in POLAN) results are good only when the true variation is approximately linear. Similarly the use of parabolic laminations (Mode 2) is satisfactory when the true gradient varies smoothly, but becomes inaccurate if the second derivative varies appreciably within one frequency interval Δf.

Errors in the linear lamination analysis can be estimated directly from the rate of change of gradient of the real-height profile (Titheridge, 1961a, Appendix). For higher order methods, however, direct calculations are difficult and relative accuracies must be determined by practical tests. Mode 1 of POLAN corresponds exactly to the widely-used linear lamination analysis. Mode 2 gives the parabolic lamination analysis; it is shown in Section 4.2 that this mode gives results which are effectively identical to those obtained from the best of the parabolic-lamination methods used by other workers. The different modes in POLAN can therefore be used to give an accurate assessment of the relative accuracy of the linear, parabolic and overlapping-polynomial techniques.

For an ionospheric real-height profile represented by $h = a + b.Fn + c.FN^2$, analysis of calculated virtual-height data gives exactly correct results (to within round-off error) for Modes 2 and above. For data corresponding to a profile $h = a + b.FN + c.FN^2 + d.FN^3 + e.FN^4$, all of the polynomial methods (Modes 4 to 9) produce the correct real heights while Modes 1 and 2 give appreciable errors. Comparison of different methods must therefore be done carefully, using profiles which cannot be represented by simple polynomial expressions. In the present work two profiles have been used to determine the relative errors of the different methods when applied to smoothly varying virtual-height data. These profiles are a parabolic layer and a Chapman layer, both with critical frequencies of 7.0 MHz. All calculations are for a dip angle of 67° and a gryofrequency of 1.2 MHz; the changes at other dip angles are considered in Appendix B.3. The following precautions were taken to avoid including errors due to starting or peak effects in the comparison.

TABLE A1. The mean absolute errors (in metres) for a parabolic layer with a scale height SH of 75 km and a critical frequency FC of 7 MHz. The means include all frequencies up to FM-3Δf (using virtual heights to FM for Mode 7, to FM-Δf for Modes 5 and 6, and to FM-2Δf for Modes 3 and 4). Values in italics give the mean error for each value of Δf, relative to Mode 2 (parabolic laminations).

Δf	FM	Mode = 1	2	3	4	5	6	7
0.1	6.85	195	1.28	0.38	0.03	0.02	0.03	0.01
	6.9	201	1.44	0.48	0.04	0.02	0.04	0.01
		146	*1.00*	*0.32*	*0.026*	*0.015*	*0.026*	*0.007*
0.2	6.7	351	3.52	2.66	0.08	0.07	0.04	0.05
	6.8	359	3.94	3.08	0.12	0.10	0.05	0.07
		95	*1.00*	*0.77*	*0.027*	*0.023*	*0.012*	*0.015*
0.3	6.6	493	6.34	4.60	0.20	0.17	0.05	0.09
	6.7	489	6.74	5.00	0.24	0.23	0.07	0.14
		75	*1.00*	*0.73*	*0.034*	*0.031*	*0.009*	*0.018*
0.4	6.4	559	8.12	5.17	0.28	0.25	0.07	0.12
	6.6	568	9.17	6.48	0.38	0.40	0.11	0.20
		65	*1.00*	*0.67*	*0.038*	*0.038*	*0.010*	*0.019*
0.5	6.3	532	8.90	6.62	0.37	0.37	0.15	0.16
	6.5	621	11.07	8.77	0.52	0.60	0.23	0.29
		58	*1.00*	*0.77*	*0.045*	*0.049*	*0.019*	*0.023*
Mean Relative:		*88*	*1.00*	*0.65*	*.034*	*.031*	*.015*	*.016*
Analysis order		1	2	3	4	5	6	7
Fitted data		1	2	3	4	6	8	11

(a) For the parabolic layer the virtual heights were calculated assuming no ionisation below the point where the plasma frequency FN = 0.9 MHz. Analysis was started from 0.9 MHz, using START = -1 in POLAN to give an accurate direct start (Section 6.2(d)), and with several closely spaced data points at the beginning to ensure that all methods began accurately. For the Chapman layer, analysis began in the linear region commencing at 2.8 MHz and used virtual-height data which ignored ionisation below this point. A direct start was again used, with the inclusion of additional data points near 2.8 MHz to ensure an accurate start for all methods.

(b) Modes 5 and 6 use virtual heights at two frequencies above the frequency at which a real height is being calculated (Figure 1 of Section 5). Mode 7 uses three such points. So to obtain an accurate comparison of the basic analysis techniques at a fixed value of Δf, unaffected by peak fitting procedures, the last three calculated heights are ignored.

Virtual heights were calculated for the parabolic and Chapman layers, for different (constant) values of the frequency interval Δf and different values of the highest frequency FM. These heights are accurate to within 0.2 metres, and involve no assumptions about profile shape. They were analysed with each of the single-step modes of POLAN (the Modes with NH = 1 in Table 1) and the absolute errors averaged to give the results shown in Tables A1 and A2.

The errors increase steadily as Δf or FM increase. The relative errors for the different methods (shown in italics, for each frequency interval Δf) show an improvement of about 90 times between the linear and parabolic lamination techniques in Table A1. A further improvement of 30 to 60 times is obtained by the use of polynomial methods. In Table A2 there is an improvement of about 50 times when going from linear to parabolic laminations and a further improvement of 10 to 30 times for the polynomial methods.

The improvement from Mode 4 to Mode 5 is often small, due to the introduction of a least-squares fit rather than an exact fit. Mode 5 fits a five-term polynomial to six data points, giving some smoothing of the data which tends to increase errors when analysing precise data. Mode 6 uses six terms fitting eight data points (Table 1 and Figure 1). It therefore gives additional smoothing in general, although the incorporation of additional constraints still gives an increased accuracy. For Mode 7 (6 terms fitting 10 constraints) the least-squares smoothing is considerable and gives a slight decrease in accuracy when analysing precise data. With normal data containing fluctuating errors, however, the smoothing is a distinct advantage and we would expect this procedure to provide the most accurate real heights.

TABLE A2. Mean absolute errors in the calculated real heights of a Chapman layer with SH = 75 km and FC = 7 MHz. Values in italics give the mean error relative to mode 2.

Δf	FM	Mode = 1	2	3	4	5	6	7
0.1	6.85	96	1.56	0.89	0.09	0.03	0.03	0.02
	6.9	101	1.76	1.25	0.11	0.03	0.04	0.02
		59.3	*1.00*	*0.64*	*0.060*	*0.018*	*0.021*	*0.012*
0.2	6.7	136	4.34	2.03	0.15	0.06	0.03	0.04
	6.8	149	4.76	2.86	0.21	0.10	0.05	0.08
		31.3	*1.00*	*0.54*	*0.040*	*0.018*	*0.009*	*0.013*
0.3	6.6	146	7.48	3.42	0.28	0.20	0.06	0.12
	6.7	166	8.37	4.31	0.36	0.30	0.09	0.19
		19.7	*1.00*	*0.49*	*0.040*	*0.032*	*0.009*	*0.020*
0.4	6.4	119	9.97	4.07	0.37	0.31	0.10	0.14
	6.6	158	12.38	6.40	0.56	0.59	0.18	0.31
		12.4	*1.00*	*0.47*	*0.042*	*0.040*	*0.013*	*0.020*
Mean Relative		*30.7*	*1.00*	*0.535*	*0.045*	*0.027*	*0.013*	*0.016*

A.2 The Analysis of Irregular Profiles

The accuracy of an N(h) analysis procedure depends on the accuracy of interpolation between real-height data points (Titheridge, 1975a). The accuracy improves (in general) as the order of the interpolating function increases, as long as instabilities are avoided. Instabilities show primarily as an oscillation in the calculated real-height points following a cusp or other discontinuity in the virtual-height data. This effect is minimised by using least-squares solutions with higher order polynomials.

The behaviour of different methods when applied to virtual-height data with cusps or other irregularities is investigated in Titheridge (1982). When the frequency interval Δf is too wide to define adequately the changes in real or virtual height, all methods give a similar smooth profile across the cusp region. As Δf decreases, however, the higher order methods give a more rapid improvement than the lamination techniques since they can more readily reproduce the inflections in the real-height profile.

Errors in the calculated profile across a cusp region give an incorrect gradient at the first frequency above a cusp. This gradient error propagates to higher frequencies in an oscillatory fashion, for all methods which require gradient continuity. The oscillations are appreciable only at the first 3 or 4 frequencies following a cusp, and are largest for the parabolic lamination procedure. The oscillations are reduced by a factor of about 1.5 for a fourth order polynomial analysis, and by a factor of about three for higher order least-squares methods. They are effectively zero for POLAN Mode 3 (as described in Titheridge, 1982).

A test profile adopted by U.R.S.I. Working Group G/6/2 (Titheridge et al., 1978) consists of two overlapping Chapman layers giving a virtual-height trace with a typical cusp. This is shown in Figure A1. Precise virtual-height data were analysed by different members using their own selection of data points and without prior knowledge of the correct result. Real heights were to be determined at a given series of frequencies; this required interpolation in the calculated real-height arrays and was designed to test accuracy at and between calculated points.

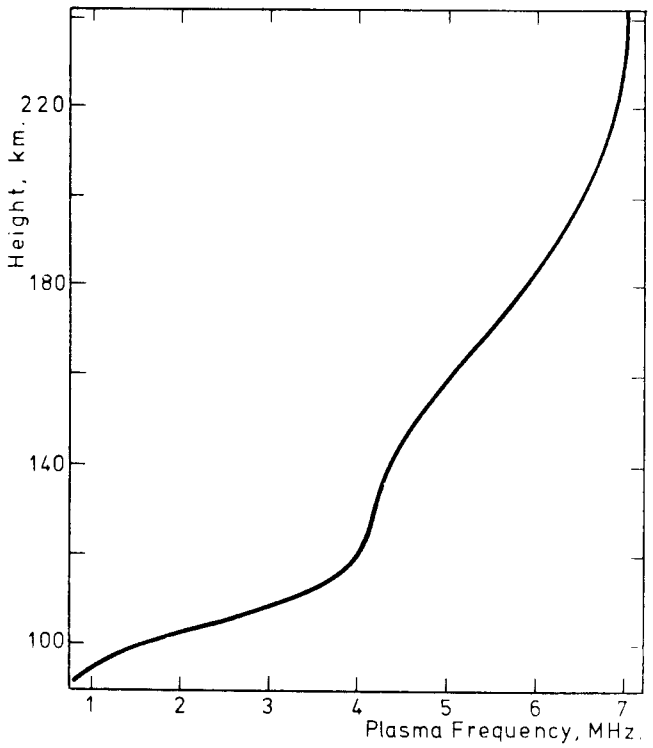

FIGURE A1. The real-height profile (consisting of two superposed Chapman layers) used to produce test ionograms with a large cusp at 4.2 MHz.

TABLE A3. The accuracy of real-height calculations for the model of Fig. A1, using 56 data points concentrated near the cusp. Errors (in metres) are for interpolated heights at 22 given frequencies, for an independent parabolic lamination analysis and for Modes 2 to 6 of POLAN.

f(MHz)	Parabolic	POLAN2	POLAN3	POLAN4	POLAN5	POLAN6
0.905	5	1	1	1	1	1 m.
1.505	20	7	7	0	0	0
2.002	19	8	9	0	0	0
2.503	15	5	6	-1	0	-1
3.004	15	5	2	-2	-1	-2
3.505	15	9	-5	-2	-1	-2
4.005	40	40	-58	-10	-3	-10
4.056	39	35	-69	-12	-5	-11
4.105	49	57	-71	-8	2	5
4.156	32	45	-32	-3	2	6
4.207	30	23	-39	-7	-3	-8
4.256	31	31	-41	-5	-2	-1
4.303	32	29	-37	-5	-3	-5
4.355	36	37	-33	-5	-4	-3
4.501	34	34	-26	-4	-3	-1
5.002	37	36	-3	-3	-1	1
5.503	39	36	-2	-3	-1	1
6.004	38	35	-10	-4	-1	-1
6.505	48	48	-36	-6	-3	-4
6.606	49	48	-33	-6	-2	-6
6.707	54	54	-30	-8	-2	-4
6.808	71	74	-28	-12	-5	-8
RMS Error =	36.9	37.1	33.6	6.0	2.5	4.9m.

The specified frequencies are given in the first column of Table A3. The next column shows the real-height errors in metres for the most successful of the parabolic-lamination results. This used minimum frequency spacings of 0.02 and 0.03 MHz across the cusp region (near 4.2 MHz). Results for POLAN Mode 2 using exactly the same virtual-height data are given in the third column of Table A3. The only consistent differences between columns 2 and 3 arise from the better start achieved by POLAN (probably due to the use of laminations parabolic in FN rather than in FN^2). Differences across the cusp region are caused entirely by the interpolation procedures. For the parabolic-lamination results, heights were obtained at the specified frequencies using the actual parabolic expressions determined for each interval. POLAN results used (in all cases) a second difference interpolation in the array of calculated real heights. This gives slightly less accuracy in irregular regions, but does not require any more information than is obtained in the calculated (height, frequency) arrays and so is the procedure normally used for determining intermediate points. If we compare heights at the frequencies used in the analysis, the parabolic-lamination and POLAN 2 results agree to within 1.5 m at all points between 4.0 and 5.0 MHz. Thus the analysis given by POLAN Mode 2 is representative of the best that can be achieved using parabolic laminations.

The RMS error for each method is given at the bottom of Table A3. By this measure POLAN 2 is identical to the parabolic lamination result. Compared with these methods the errors are smaller by a factor of 5 for POLAN 4, and a factor of 10 for POLAN 5. Maximum errors in the cusp region are reduced by a factor of 2 or 3 for POLAN 4, and 4 or 5 for POLAN 5. For POLAN 6 (which fits a 6-term polynomial to 8 data points) the increased smoothing given by the least-squares fit leads to increased errors in the region of greatest curvature (just below the cusp). This smoothing will, however, be an advantage in the presence of typical fluctuating data errors. [Note that Modes 4 to 6 were labelled 3 to 5 in the original test, and errors from 4.25 to 4.5 MHz were appreciably greater since POLAN then used only a linear-lamination approximation for underlying sections rather than the procedure described in Appendix D.2.]

Results obtained by analysing the same virtual-height profile using different, constant values of the frequency interval Δf are shown in Table A4. The errors given here are the mean absolute value and the RMS value of the errors at equally spaced data frequencies, from 1.0 to 6.8 MHz inclusive. Largest errors occur near the cusp, in all cases, since errors near the peak (at frequencies up to 6.8 MHz) are reasonably small with these values of Δf. The RMS error reflects primarily the maximum errors in the cusp region, while the mean error includes a larger contribution from the post-cusp error.

TABLE A4. The error in metres obtained by analysing virtual-height data for the profile of Figure A1, at a dip angle of 67°, for three different values of scaled frequency interval Δf. Solid type gives the mean absolute error, and the RMS error, from 1.0 to 6.8 MHz inclusive. Values in italics show the average of the Mean and RMS values, relative to the results for Mode 2 (parabolic laminations).

POLAN Mode =	1	2	3	4	5	6	7
$\Delta f=0.1$							
Mean:	353	63.6	31.6	16.9	19.8	16.7	39.4
RMS:	491	80.8	54.3	40.3	36.2	28.7	76.9
Relative:	*5.84*	*1.00*	*0.59*	*0.40*	*0.39*	*0.31*	*0.80*
$\Delta f=0.05$							
Mean:	223	25.2	13.7	5.5	7.3	6.6	5.7
RMS:	305	28.5	21.0	9.1	11.9	11.2	9.3
Relative:	*9.83*	*1.00*	*0.65*	*0.27*	*0.36*	*0.33*	*0.28*
$\Delta f=0.025$							
Mean:	306	25.3	20.1	3.7	2.3	2.4	2.9
RMS:	393	30.5	27.8	4.9	3.8	3.8	4.8
Relative:	*12.53*	*1.00*	*0.86*	*0.15*	*0.11*	*0.11*	*0.14*

All errors in Table A4 are appreciably less for the higher order methods. The difference is least at $\Delta f = 0.1$ MHz, where the given data is insufficient to define the real-height variations and all methods give a smoothed profile. At smaller values of Δf the higher order methods improve more rapidly, showing the greater ease with which they follow complex profile variations. We therefore conclude that the analysis order represented by POLAN Mode 5 or Mode 6 gives an appreciable improvement on procedures currently in use (which correspond to Modes 1 and 2), for both smooth and irregular profiles, at large and small scaling intervals. The overlapping-cubic procedure (Mode 3) eliminates any oscillatory tendencies with irregular profiles. Such tendencies are, however, quite small with the higher order polynomials. The higher modes are therefore generally preferred.

A.3 The Effect of Errors in the Virtual Height Data

(i) Basic errors in virtual height

There are several possible sources of error in the basic relation giving h' as an integral of $\mu' dh$. Even in the absence of collisions, the ray theory assumed becomes inapplicable near the peak of a layer; the errors are however appreciable only within about 0.01% of the critical frequency, and so are of little concern.

Collisions made by electrons in the ionosphere reduce μ' in the region near reflection, and can considerably decrease the height h' obtained by a direct integration of the real part of μ'. Under these conditions, however, μ is not zero at any real height and ray theory fails. In the absence of a magnetic field, and replacing the true profile by a linear approximation near reflection, integration in the complex plane shows that collisions have zero effect on the true value of h' (Titheridge, 1961b). Numerical calculations show that this result is generally applicable. An exact virtual height is obtained by integrating the complex value of μ', including the collision terms, up to the complex height at which $\mu' = 0$. At all dip angles this gives, to within 0.1%, the same result as integrating the no-collision expression for μ' up to the classical reflection height (Titheridge, 1967a). The effect of collisions should therefore be ignored at all stages in the analysis.

A further assumption inherent in the expression for h', that of a vertically propagating ray, can cause considerable errors. With an inclined magnetic field the O and X rays are deviated horizontally in opposite directions through a distance of typically 20 km (Titheridge, 1959a). The horizontal displacement is largest in the F region, so that the value of foF2 measured at mid latitudes commonly applies to a point about 40 km polewards of the observing site. This deviation does not affect the virtual heights for a horizontally stratified ionosphere, when the wave-normal remains vertical

throughout. Errors will occur, however, if the ionosphere is not horizontally uniform, and detailed comparisons of h'x and h'o to obtain information about the unseen regions will become unreliable.

The presence of large irregularities in the ionosphere can cause horizontal deviations of over 100 km (Lobb and Titheridge, 1977b). The rays avoid regions of decreased density, so a decrease travelling over a station may pass unseen on the ionograms. A similar increase will appear perhaps 200 km larger (horizontally) than its true dimensions. In either case, when there is an irregularity within a few hundred km of the station, ionograms do not give a reliable measure of even the overhead critical frequency. Ray-tracing calculations show that, in the presence of a wave-like disturbance, ionogram analysis gives most nearly the profile of the undisturbed ionosphere.

Experimental limitations restrict the accuracy of measured virtual heights. Serious errors arise from the effect of pulse delay in the receiver, and from changes in the width of the recorded trace with echo amplitude. Since measurements are normally made to the leading edge of the echo, these effects cause the measured heights to be too large and to vary irregularly by as much as 10 or 20 km. Many ionograms have a zero error of about 10 km, due to delay in the receiver; this error can be determined by comparing the heights of multiple reflections. The effect of variations in the width of the h'(f) trace has been studied, for a particular ionospheric recorder, by Lyon and Moorat (1956). They found that the height measured to the leading edge of the echo changed by about one quarter of the total change in the echo width. For other ionosondes the change in the position of the leading edge may be as much as half the change in the width of the recorded trace (e.g. Koehler and McNamara, 1975). For accurate results this variation should be determined and a corresponding correction made when scaling the virtual heights.

The size of typical virtual-height errors $\Delta h'$ has been considered by Koehler and McNamara (1975). Uncertainties in the correction for receiver delay, and in the zero height correction, produce virtual-height errors of about ± 1 km for strong echos and ± 2 km for weak echos. The errors become largest where the virtual heights are changing most rapidly, through increased difficulty in defining the leading edge of the echo and because small errors in frequency give large errors in the corresponding virtual heights. The uncertainty in scaled frequencies is commonly 1 or 2 percent of the frequency. Using cross-wires locked in the frequency direction, repeated scaling of the same point by different persons showed random variations in virtual height (with two typical ionograms) through a range of about $0.5 + 0.001(dh'/d\ln f)$ km, where $\ln f$ is the natural logarithm of the frequency in MHz. Errors in scaling the positions of the frequency markers add a further uncertainty of perhaps 0.1% in the frequency axis, corresponding to a virtual-height error of about $0.001(dh'/d\ln f)$ km.

An exercise carried out within U.R.S.I. W.G. G/6/2 consisted of scaling a good-quality midlatitude ionogram by different members. Results showed variations in virtual height of ± 2 km in the E region and ± 5 km in the F region, where the virtual-height trace was approximately horizontal. The variations increased near critical frequencies. Thus for typical ionograms and good quality echos we expect overall fluctuations in virtual-height, due to scaling errors, of roughly

$$\Delta h' \simeq 2.0 + 0.001(dh'/d\ln f) \text{ km in the E region,} \qquad (A1)$$

and

$$\Delta h' \simeq 4.0 + 0.002(dh'/d\ln f) \text{ km in the F region.} \qquad (A2)$$

The gradient $dh'/d\ln f$ is typically about 5000 km near a cusp, giving RMS errors in virtual height of 3 to 10 km. Data acquired directly from modern digital ionosondes will eliminate most of these scaling errors, although changes in echo amplitude may still give spurious changes in the recorded virtual heights with some instruments.

(ii) **Resulting errors in the real height**

The accuracy of a calculated N(h) profile depends on the amount and accuracy of the given virtual-height data and on the accuracy of the N(h) analysis procedure. It can be shown (Titheridge, 1975a) that errors in the given virtual heights produce approximately the same changes in the calculated real heights for all methods of analysis. Using a frequency spacing Δf of 0.2 MHz, an isolated error $\Delta h'$ in one virtual height produces a real-height error Δh with a mean value of about $0.06\Delta h'$, at about 10 successive frequencies. For different values of Δf, the errors were found to vary approximately as $\Delta f^{0.6}$. The real-height error Δh is therefore

$$\Delta h \simeq 0.06\,\Delta h' \,(\Delta f/0.2)^{0.6}$$

averaged over about 10 successive points. For random errors $\Delta h'$ on all virtual heights, the mean value of Δh will increase about 3 times. Thus for any method of N(h) analysis, random errors of $\Delta h'$ km in the virtual-height data produce real-height errors of the order of

$$\Delta h \simeq 0.5\,(\Delta f)^{0.6}\Delta h'. \qquad \text{(A3)}$$

For typical virtual-height errors of about 2.5 km (RMS), and frequency intervals Δf of 0.1 MHz, (A3) indicates fluctuating real-height errors of about 0.3 km.

Calculated profiles also include a larger but more slowly-varying error due to uncertainties in the start and valley corrections. The effect of random errors on the start calculation is considered in Appendix B.2. For virtual-height errors of about 2.0 km, the RMS error in the calculated starting heights is about 5 km at dip angles less than 32°, and 10 km at dip angles above 40°. (The errors become very large at dip angles near 35°, as shown in Fig. B4, when combined O and X ray calculations for the unobserved regions become impractical.) For valley calculations the same virtual-height errors give a RMS real-height error of about 15 km, just above the valley (Appendix B.2). These are fundamental errors which will occur in all calculations, using a purely mathematical procedure based on combined O and X ray data. Biasing of the results by the inclusion of suitably weighted physical constraints in a least-squares analysis (as described in Sections 7.3 and 8.4) commonly reduces the real-height fluctuations by a factor of about 2.

The errors introduced by incorrect start and valley corrections vary smoothly with frequency. Continuous lines in Fig. A2 show the change Δh in real height, as a function of the plasma frequency f (expressed as a fraction of the gyrofrequency FH), for a change of 5 km in the assumed real height at f = 0.5FH. Adding (or subtracting) any multiple of these curves from a profile does not alter the virtual heights for the O ray. Figure A2 can therefore be used to determine the changes in real height, at any frequency, caused by a change in the assumed size of the starting correction. As shown by the broken line, the real-height changes decrease approximately as 1/f at increasing frequencies.

Corresponding results for the valley correction are given in Fig. 9 of Section 7.4. Changes in the real height of the upper layer, due to changes in the assumed width of the valley region, vary approximately as $1/f^2$ at frequencies near the critical frequency FC of the underlying peak. At higher frequencies, greater than about 2FC, the real height changes vary approximately as 1/f.

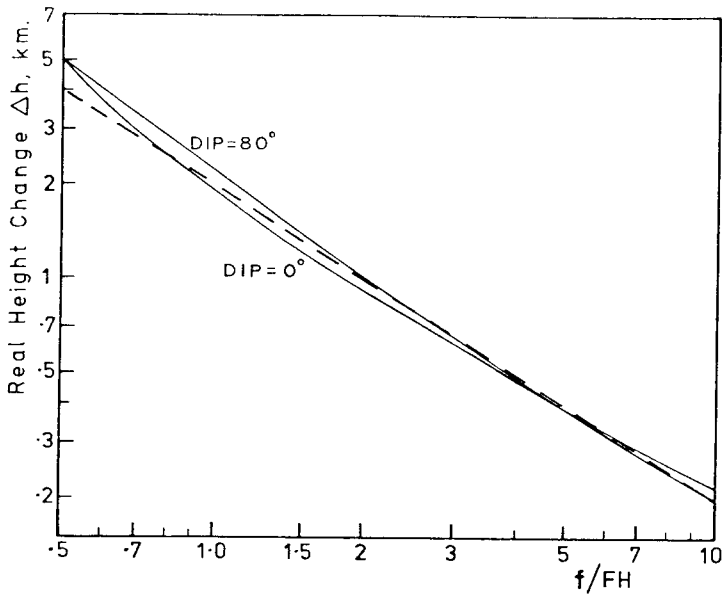

Figure A2. Changes in real height, beginning at a frequency f of half the gyrofrequency FH, that produce no change in the virtual height of the ordinary ray. Results are shown for dip angles of 0° and 80°, assuming a change of 5 km in the real height at plasma frequencies of 0 to 0.5FH.

APPENDIX B. DEPENDENCE OF THE GROUP REFRACTIVE INDEX ON DIP ANGLE.

B.1 Values of group index

The group refractive index μ' varies only slowly with the plasma frequency FN when FN is small, but $d\mu'/dFN$ increases rapidly near the reflection point and becomes infinite at FN = FR. Changes in μ' are therefore displayed more clearly if we use a variable T defined by

$$T^2 = 1 - FN^2/FR^2. \qquad (B1)$$

For the O ray at a dip angle I = 0°, $\mu'T$ is constant and equal to 1. dT/dFN is proportional to 1/T and, under all conditions, tends to infinity at reflection (where T = 0) in the same way as $d\mu'/dFN$. Thus $d\mu'/dT$ is finite and well-behaved throughout.

For dip angles of 20°, 50° and 80° the ratio $(\mu'_X - 1)/(\mu'_O - 1)$ is shown as a function of T in Fig. B1. The values of μ' are for 'corresponding' O and X rays, with the same plasma frequency FR at reflection. Thus the curves in Fig. B1 give the ratio of the group retardations of corresponding X and O rays, from the base of the ionosphere (T = 1) to the reflection point at T = 0. For a given dip angle, values of μ' depend only on the ratios of the frequencies FN, FR and FH. FN/FR is specified by T, while FR/FH appears as an independent parameter.

At a dip angle of 80° (the broken lines in Fig. B1) the group retardation ratio

$$R_{X,O} = (\mu'_X - 1) / (\mu'_O - 1)$$

varies considerably from T = 1 to T = 0. Throughout most of the range $0 < FN < 0.98FR$ (corresponding to $T > 0.2$) the ratio $R_{X,O}$ is large, with a comparatively constant value of about 2.3, 4.0 or 6.0 at FR/FH = 4, 2 or 1.4 respectively. Thus the ratio of the retardations for the X and O rays is roughly constant and proportional to FH/FR at $FN < 0.98FR$. The ratio passes through unity near FN = 0.99FR, corresponding to T = 0.13. For values of FN between 0.995FR and the reflection point FN = FR (the range 0.1 to 0 in T), $R_{X,O}$ has a mean value of about 0.4 for all values of FR/FH.

At dip angles near 80° we therefore have two distinct regions causing differential retardation of the O and X rays.

(a) For plasma frequencies FN within 0.5% of the value FR for reflection, the group retardation of the X ray is about 0.4 times that of the O ray. The gradient at reflection therefore causes about 2.5 times as much group retardation for the O ray as for the X ray.

(b) For plasma frequencies $FN < 0.98FR$ the group retardation of the X ray over the region $0 < FN < 0.98FR$ is approximately 4 times that of the O ray. Underlying ionisation therefore causes a large increase in h'_X and a considerably smaller change in h'_O.

Observed values of h'_X and h'_O can give no information about the distribution of ionisation in any region where $R_{X,O}$ is approximately independent of FN. Thus if $R_{X,O} \simeq \bar{R}$ in a region $F1 < FN < F2$, the group retardation of the X ray in this region is:

$$Dh'_X = \int_{F1}^{F2} (\mu'_X - 1)\,(dh/dFN).dFN \simeq \bar{R} \int_{F1}^{F2} (\mu'_O - 1)\,(dh/dFN).dFN$$

or

$$Dh'_X \simeq \bar{R}.Dh'_O \,. \qquad (B2)$$

Changes in profile shape which do not alter the value of

$$Dh'_O = \int_{F1}^{F2} (\mu'_O - 1)\,(dh/dFN).dFN$$

will not alter the value of Dh'_X, and so they are not detectable. The ratio $R_{X,O}$ may vary with frequency, i.e. with the value of FR. As long as it is approximately independent of FN over the region $F1 < FN < F2$, however, changes in Dh'_X are related to those in Dh'_O by the known constant $\bar{R}$. Measurements of h'_X then give no additional information.

The curves in Fig. B1 show that $R_{X,O}$ is approximately independent of T for $T > 0.7$, corresponding to $FN < 0.7FR$. This is true for all frequencies at dip angles less than 30° or greater than 60°. At intermediate dip angles it is true for frequencies FR greater than 2FH. Under these conditions, and taking FR as the minimum observed frequency fmin, no information about the distribution of ionisation in the region $FN < 0.7fmin$ can be obtained from the observed O and X ray

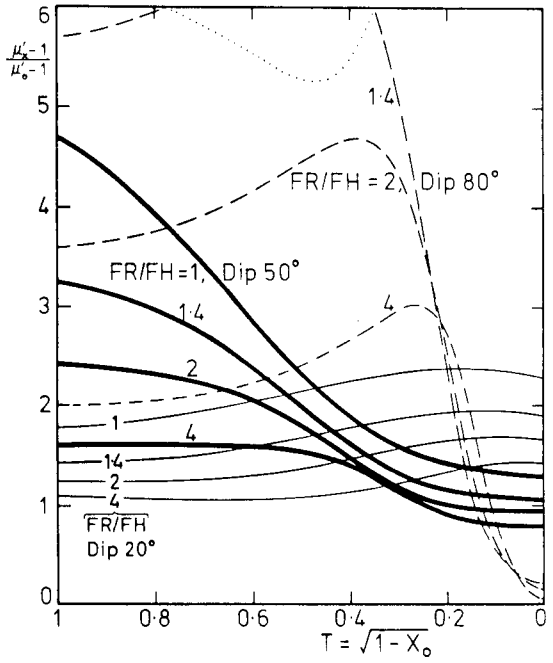

Figure B1. The relative group delays of the extraordinary and ordinary rays from the base of the ionosphere (T = 1) to reflection (T = 0). FR is the plasma frequency at reflection for both X and O rays. FH is the gyrofrequency.

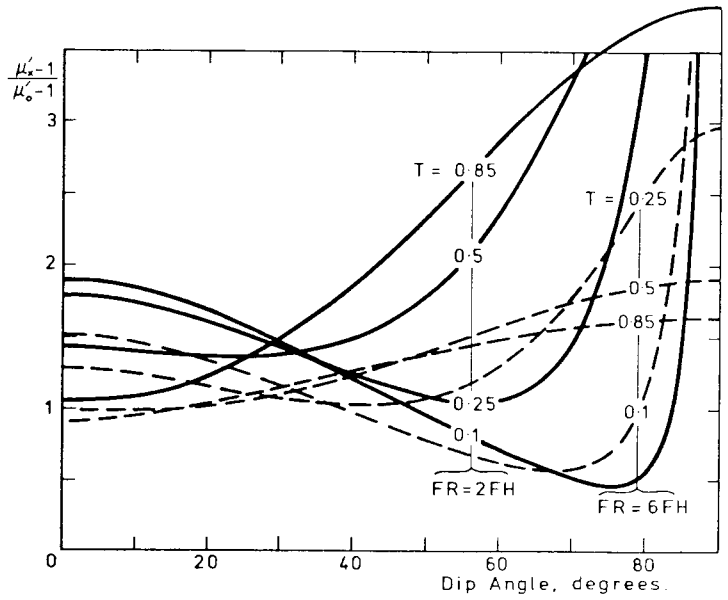

Figure B2. The group delay ratio $R_{X,O} = (\mu'_X - 1)/(\mu'_O - 1)$ as a function of dip angle, for plasma frequencies at reflection (FR) of twice and six times the gyrofrequency. The curves at T = 0.85, 0.5, 0.25 and 0.1 correspond to FN/FR = 0.53, 0.87, 0.97 and 0.997 respectively.

virtual heights. This is true for any method of analysis. Thus a basic requirement for a stable analysis procedure is that it should not attempt to determine the distribution of ionisation in this region.

Figure B2 shows the variation of $R_{X,O}$ with dip angle for 4 fixed values of T, corresponding to plasma frequencies of 0.53, 0.87, 0.97 and 0.995 times FR. Solid lines are for typical start calculations, with FR = 2FH. The broken lines, for FR = 6FH, are typical of valley calculations. In both cases $R_{X,O}$ increases with increasing FN (decreasing T) at $I < 30°$; decreases with increasing FN from 30° to 70°; and increases with increasing FN at dip angles above about 85°. Thus for dip angles of 0 to 20°, $h'_X - h'_O$ is increased most by high density ionisation. This is also shown in Fig. B1, where the ratio $R_{X,O}$ increases as T tends to zero at dip 20°. At $I > 40°$ the values of $h'_X - h'_O$ are increased by low density ionisation only. Thus in Fig. B1, $R_{X,O}$ is greater than 1.5 for all $T > 0.4$ ($FN < 0.92FR$) at 50° dip, and for all $T > 0.15$ ($FN < 0.99FR$) at 80° dip.

One anomalous point apparent in Fig. B2 is at a dip angle of 30°. Here the ratio $R_{X,O}$ is approximately constant, at a given frequency, for all values of T. Thus we have $R_{X,O} = 1.44 \pm 0.06$ at FR = 6FH. For rays reflected at FN = FR = 2FH the total delays $D = h' - HR$ are related by $D_X = (1.44 \pm 0.06)D_O$. The real height HR at the plasma frequency FR is then

$$HR = h'_O - (h'_X - h'_O)/(0.44 \pm 0.06).$$

At dip 30° observed virtual heights therefore give directly the real heights of reflection (Titheridge, 1974b). The total delay $h' - HR$ is also obtained in one step which involves no assumptions or calculations relating to the distribution of the underlying ionisation. It follows that no information can be obtained about the distribution of the underlying ionisation, at a dip angle of 30°. Using the argument following equation (B2), $R_{X,O}$ is constant for all FM < fmin so that the region in which values of (dh/dFN) can not be found extends right up to the lowest observed frequency fmin. A severe practical limitation also occurs near dip 35° (as in Fig. B4).

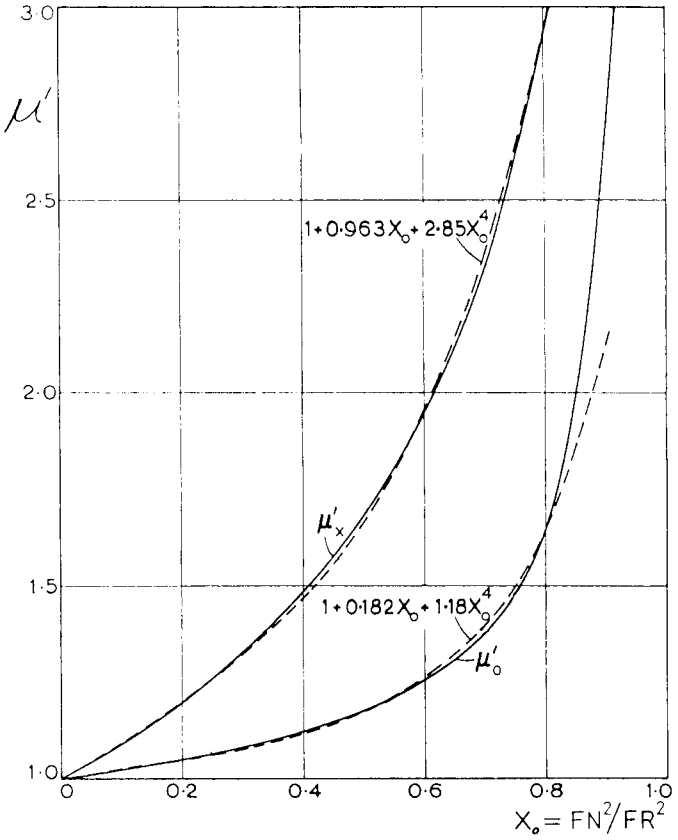

Figure B3. Values of the group refractive indices μ'_X and μ'_O at I = 67° and FH = 1.18 MHz. μ' becomes infinite at the reflection point where $X_O = 1$. Broken lines show 3-term polynomial approximations, accurate to within 5% for $X_O < 0.84$.

B.2 Information obtainable using O and X rays

We have seen above that information about the distribution of unseen ionisation cannot be found over any range of plasma frequencies FN for which the ratio $R_{X,O} = (\mu'_X - 1)/(\mu'_O - 1)$ is approximately constant. At all dip angles this range includes the region FN = 0 to FN = 0.7fmin, for fmin > 2FH. At most dip angles $R_{X,O}$ is approximately constant over the range 0 < FN < 0.7fmin for all frequencies down to 1.0FH, so that the distribution of ionisation is never obtainable at FN < 0.7fmin. An exception occurs for dip angles near 50° (Fig. B1), when dR/dT is quite large down to T = 1 at FR ≃ FH. Observed virtual heights then depend on the distribution of ionisation down to quite low values of FN/fmin, and good observations could be used to determine this distribution.

Although (in general) the actual distribution of ionisation cannot be found at FN < 0.7fmin, the overall effect of this region is measureable. The solid lines in Fig. B3 show the variation of μ' with X_O for FR = 1.7FH at dip 67° (from Titheridge, 1959b). Broken lines show approximating expressions of the form

$$\mu' = 1 + aX_O + bX_O^4, \qquad \text{where} \qquad X_O = FN^2/FR^2 \quad \text{in (B1).}$$

These approximations have a maximum error of 5% for values of X_O up to 0.84, corresponding to FN = 0.917FR. The error is generally much less than 5%, and is of changing sign. Thus for both O and X rays the overall group delay due to any region with FN < 0.9fmin is given to within about 1% by

$$D = \int_0^{0.9fmin} (\mu' - 1)(dh/dFN).dFN \tag{B3a}$$

$$= A\int_0^{HA} FN^2.dh + B\int_0^{HA} FN^8.dh \tag{B3b}$$

where $A = a/FR^2$, $B = b/FR^8$ and HA is the height at which FN = 0.9fmin. The functions a, b, A and B vary with frequency (i.e. with FR), but do not depend on the gradient dh/DFN in the region FN < 0.9fmin. Thus the only information which can be obtained about this underlying region is the values of $\int N dh$ and $\int N^4 dh$, where N is the electron density (proportional to FN^2).

The effect of errors in the virtual-height data can be calculated directly, and is independent of the shape of the real-height profile. Suppose that exact virtual heights h'_i produce real heights h_i. The analysis corresponds to a matrix transformation of the type

$$\mathbf{[H]} = \mathbf{[M]}.\mathbf{[H']} \tag{B4}$$

where **[H']** is a column matrix giving the virtual-height data and **[H]** is the array of real heights. This applies to exact and least-squares solutions, with a single component or with both O and X-ray data. The matrix **[M]** is independent of the data and involves only the frequencies used and the magnetic field constants.

Changes Dh' in the virtual heights produce changes Dh in the real heights, related by

$$\mathbf{[DH]} = \mathbf{[M]}.\mathbf{[DH']}. \tag{B5}$$

Thus real-height errors are a linear function of the virtual-height errors. An error matrix E(i,j) can be derived which gives the real-height error at a frequency f_i, due to an error e_j in the virtual height h'_j, as

$$Dh_i = E(i,j)\, e_j. \tag{B6}$$

This means that an error of 1 km in the virtual height at the jth data frequency produces an error E(i,j) km in the ith real height. If each of the n virtual-height data points has a similar random error, with a RMS value <e>, the RMS real-height error is

$$Dh_i = E_i.\langle e\rangle \tag{B7a}$$

where

$$E_i^2 = \sum_{j=1}^{n} E(i,j)^2 \tag{B7b}$$

Error matrices were obtained for slab start calculations using a 5-term real-height polynomial (POLAN mode 5), with 5 O-ray and 5 X-ray data points at a frequency spacing of 0.1 MHz. Errors in the calculated real-height profile, at two points in the unobserved range and one in the center of the observed range, are listed in Table B1. Mean real-height errors near the center of the scaled

frequency range, and averaged over both ranges of dip angle in Table B1, are typically as shown below where $\langle e_0 \rangle$ and $\langle e_x \rangle$ are the RMS errors in the O and X ray virtual-height data.

For Start calculations with fmin $\simeq$ FH:

$$\begin{aligned} Dh &\simeq 3.0 \langle e_0 \rangle \quad \text{for O-ray errors only} \\ Dh &\simeq 2.0 \langle e_x \rangle \quad \text{for X-ray errors only} \end{aligned} \tag{B8}$$

and

$$Dh \simeq 3.0 \langle e \rangle \quad \text{at } \langle e_0 \rangle = \langle e_x \rangle = \langle e \rangle \tag{B9}$$

If the virtual heights contain systematic errors, of e_0 km for the O-ray data and e_x km for the X-ray data, these give a real-height error of

$$Dh \simeq 3.5e_0 - 2.5e_x. \tag{B10}$$

At dip angles near 35° the matrix [M] in (B4) becomes ill-conditioned. This occurs because the variations of μ'_x and μ'_0 with plasma frequency FN are very similar in shape at different frequencies. Small changes in the virtual heights then produce large changes in the real heights. Figure B4 shows the value of E_i defined by (B7), for a frequency f_i in the center of the scaled frequency range, plotted as a function of dip angle. A solid bar marks the region at dip angles of 33° to 38°. Over this range the presence of even small errors in the virtual-height data makes useful start calculations impossible.

The same problem is encountered for valley calculations, using combined O and X ray data, at dip angles near 35°. This is indicated in Fig. 21 (Section 9.4) where changes in the assumed valley depth produce increased fluctuations in the calculated profile near DIP = 35°, even with exact data. For valley calculations the frequencies used are well above the gyrofrequency, so the difference between O and X-ray data decreases. This gives an increased sensitivity to data errors at all dip angles. When the critical frequency of the underlying (E layer) peak is about 3.0 MHz, the real-height errors just above the valley (due to virtual-height errors with a RMS value $\langle e \rangle$) are typically

$$\begin{aligned} Dh &\simeq 6 \langle e_0 \rangle \quad \text{for O-ray errors only} \\ Dh &\simeq 5 \langle e_x \rangle \quad \text{for X-ray errors only} \end{aligned} \tag{B11}$$

and

$$Dh \simeq 8 \langle e \rangle \quad \text{at } \langle e_0 \rangle = \langle e_x \rangle = \langle e \rangle \tag{B12}$$

For both start and valley calculations, data errors have least effect on the calculated profile (in the observed range) at dip angles near 29°. This occurs even although little information can be found about the unobserved regions, as discussed in Section B.1.

Table B1. Errors in the calculated real-height profile, due to random virtual-height errors with a RMS value of 1.0 km. Results are for a slab start calculation using combined O and X ray data. Values shown are the RMS error in the thickness of the underlying slab of ionisation (q(MT) in Fig. 10 of Section 8.3); in the start offset (giving the real height at a frequency of 0.6fmin); and in the real height at the center of the scaled frequency range. These values are approximate mean errors over the indicated range of dip angles.

Calculated quantity	DIP < 27°	DIP > 40°	
Slab thickness q(MT)	31.	33.	km
Start offset q(MT+1)	8.	13.	km
Real height in center of range	2.5	5.	km

B.3 The reduction of integration errors at high dip angles

In the calculation of virtual-height integrals, maximum accuracy is obtained using the relation

$$h' = h + FR \int (1/FN)(dh/dFN).(\mu'T-T)\, dT \qquad (B13)$$

where T is defined by (B1), FR is the plasma frequency at reflection, and dh/dFN is the profile gradient. The value of T ranges from 1 at FN = 0 to zero at reflection (where μ' is infinite). For dip angles less than 90° the value of $(\mu'T-T)$ is finite throughout, and for I < 60° it is a smoothly varying function of T. The value of $\mu'T$ is equal to secI at reflection, and becomes infinite at I = 90°. The rapid increase of $\mu'T$ is confined to very small values of T when I is near 90°, as shown in Fig. B5.

Most of the group delay occurs in a small interval near reflection, with FN and (dh/dFN) not changing rapidly. The integral in (B13) is then proportional to the area under the curves in Fig. B5, from $T = TB = (1 - FA^2/FR^2).5$ (where FA is the lowest plasma frequency included in the integration) to the reflection point at T = 0. With the large, rapid increase near T = 0 even the 12-point Gaussian integration in POLAN becomes increasingly inaccurate from I = 67° to I = 79°, and normal integration techniques are useless at I = 89°. This is shown in Fig. B6, which gives the errors involved in analysis of a smooth virtual-height curve. With 5-point integrals (the broken lines in Fig. B6) errors increase rapidly at dip angles above 45° for the overlapping-polynomial methods, above 65° for parabolic laminations, and above 80° for linear laminations. Using 12-point integrals the basic accuracies are maintained to dip angles of about 80, 84 and 87° respectively. At dip angles above 85° the limitations of a 12-point integral cause the high order polynomial methods to give the same mean error as the parabolic-lamination method.

Integration accuracy is improved at large dip angles by dividing the integration range into two sections. The vertical lines in Fig. B5 indicate the approximate boundary between the slowly-varying and rapidly-increasing sections of the curves. To the left of these lines, adequate accuracy can be obtained with a 12-point Gaussian integral. The section to the right has a very large increase in $(\mu'T-T)$ at large dip angles. This increase corresponds roughly to a symmetrical S-shaped variation, with approximately equal gradients at each end. This form is reliably evaluated by standard methods of integration. The main requirement for accuracy is that the errors due to the sharply-curved sections at the two ends must be approximately equal and opposite. The positions of the vertical lines in Fig. B5 were estimated to fulfil this requirement. Calculations were then carried out using

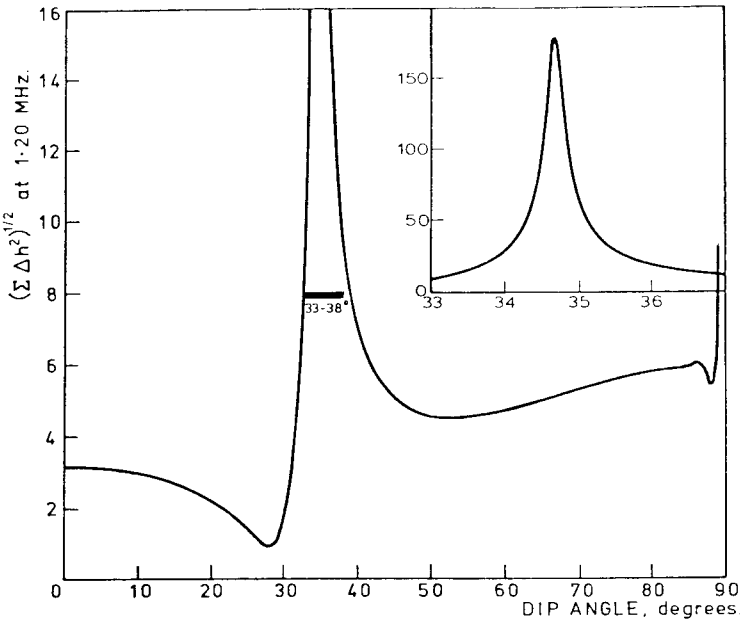

Figure B4. The RMS real-height error produced by random virtual-height errors with a RMS value of 1 km. Results are for a slab start calculation using 5 O-ray points at frequencies of 1.0FH to 1.4FH, and the corresponding X-ray frequencies (reflected at the same real heights).

5-point Gaussian integration for $T > TC$ and 12-point integration for $TC > T > 0$, adjusting the value of TC to obtain the minimum overall error. The minimum is reasonably broad, and variations of up to 10% in TC (from the optimum value) cause little increase in the overall error. The optimum values of TC change by only about 10% for different frequencies in the range 1 to 15 MHz, so a mean value can be used for all frequencies at a given dip angle. The optimised mean values are given to within a few percent by the relation

$$TC = 0.39 - 0.05 \sec(0.016I) \qquad (B14)$$

where the dip angle I is in degrees, and $0.016I$ is in radians.

Implementation of the 17-point integration in the subroutine COEFIC is straightforward. The Gaussian coefficients T_r and the corresponding weights W_r are stored in 17-point arrays TR and W. The first 5 array elements are for the 5-point integrals used with MODE = 1 to 7, and the following 12 are for the 12-point integrals used at MODE = 8 to 20 (Appendix D.1). For a 17-point integral, all coefficients are used in succession; the limits on T being changed from TB, TC for the first 5 evaluations of $(\mu'T-T)$ to TC, 0 for the following 12 evaluations. This dual integration is used automatically by COEFIC when

(i) a 12-point integration was originally specified (for accurate results);
AND (ii) the dip angle I is greater than or equal to 60°;
AND (iii) the value of TB is greater than 1.2TC.

Results for the parabolic layer are shown by the dotted lines in Fig. B6. Use of the dual (17-point) integration reduces errors in the polynomial methods by a factor of about 10 to 100 at dip angles of 80 to 88°, and reasonable results can be obtained for dip angles as high as 89°.

For the extraordinary ray $\mu'T$ varies smoothly with T and 5- or 12-point integrals are adequate at all dip angles. For combined O and X ray analyses, as used to resolve the starting and valley ambiguities, use of the 17-point O-ray integral gives no increase in overall errors at any dip angle. This is clearly demonstrated by the results of Fig. 21 (Section 9.4), which maintain good accuracy in the calculation of valley size at all dip angles up to and including 90°. To attain such results the calculation of $\mu'T$ must be free of small difference errors at all values of T (in 0.0 to 1.0 inclusive) for dip angles up to $I = 90°$. A straightforward formulation which fully meets this requirement is provided by the subroutine GIND described in Appendix D.3.

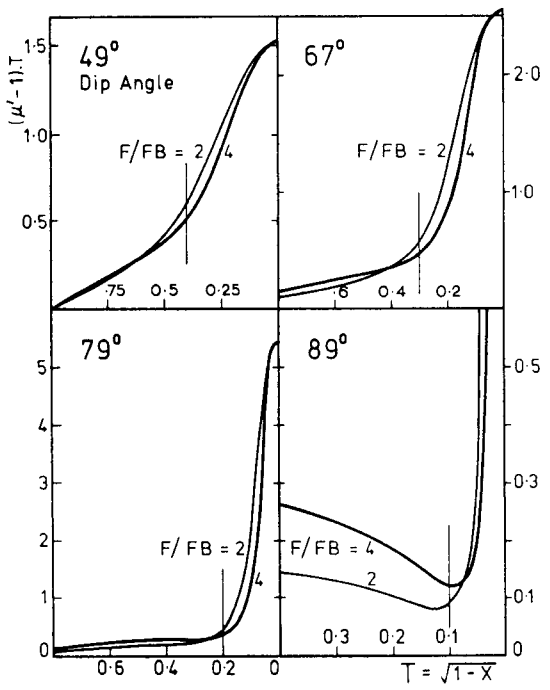

Figure B5. $\mu'T - T$ plotted as a function of T, for dip angles I corresponding to $\sec(I/2) = 1.1, 1.2, 1.3$ and 1.4. Thin and thick lines are for frequencies of 2 and 4 times the gyrofrequency FB. Vertical lines indicate the point $TC = 1.5 - \sec(I/2)$ at which the range of T is divided for integration.

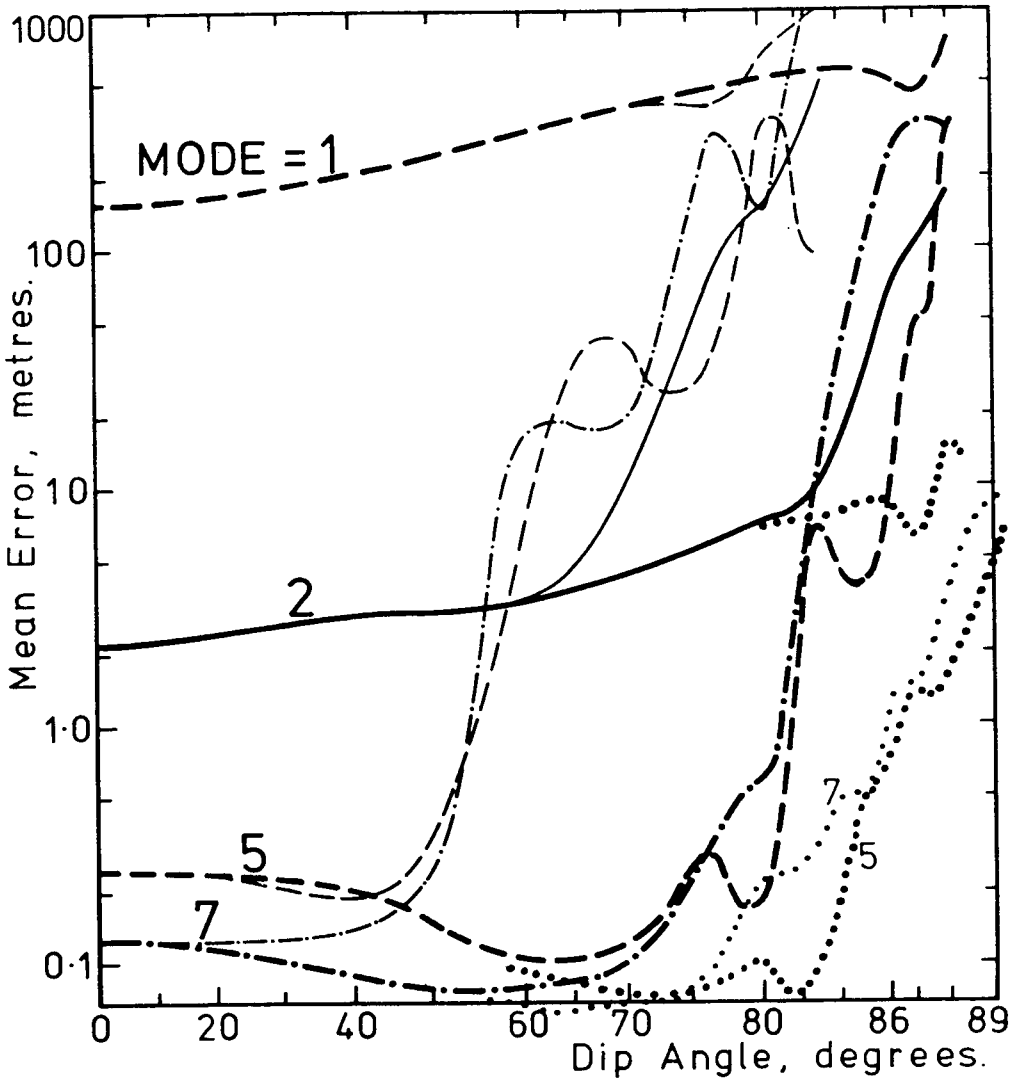

Figure B6. The mean error in the real heights calculated from exact virtual height data, at a frequency interval of 0.2 MHz, for a parabolic layer with a scale height of 60 km and a critical frequency of 7.0 MHz. Results shown are for 4 modes of POLAN, using 5-point (fine lines) and 12-point (heavy lines) integration. Dotted lines show results from the two-stage integration developed for increased accuracy at high dip angles.

APPENDIX C. THE EFFECTS OF A VARYING GYROFREQUENCY

C.1 Values of gyrofrequency in the ionosphere

Satellite measurements show that the magnetic field strength in the ionosphere is normally within 1% of the value obtained by inverse-cube extrapolation of ground measurements. For vertical propagation we may therefore assume a constant dip angle and a gyrofrequency

$$FH = FB/(1 + h/6371.2)^3 \qquad (C1)$$

where FB is the ground value and h is the height in km.

Values of FH can be obtained from ionograms by comparing the O and X ray frequencies corresponding to a cusp or critical frequency. 500 accurate E region records taken at Cambridge by Robinson (1958) were examined for this purpose. In 76 cases, corresponding cusps or discontinities could be clearly recognised for both O and X rays. The results, shown in Fig. C1(a), give a mean value FH = 1.20 with a standard error of 0.01 MHz. Calculations using field-strength measurements from nearby observatories give FH = 1.26 MHz at 110 km, the approximate height of the E layer reflections. Thus the values of gyrofrequency needed to match ionogram obserations show a scatter of about 5%, and a mean error of about 5% with respect to absolute calculations. The scatter shows that, with high quality ionograms, errors of at least 1% are normal in scaled critical frequencies.

Figure C1(b) shows values of FH derived from careful F-region measurements at Brisbane, corrected for the effect of horizontal gradients (Ellis, 1957). The mean result is 10% above a dipole field fitted to ground measurementts. Making allowance for underlying ionisation in the profile calculations could reduce the difference to about 6%. This minimum discrepancy corresponds to a consistent error of at least 1% in the measurements of critical frequency. These "errors" may be due to gradients and irregularities in the ionosphere. They set a limit on the accuracy of profile calculations using combined O and X ray data, which require accurate identification of "corresponding" O and X frequencies.

Start and valley calculations rely on the difference in virtual height of O and X rays reflected at the same true height. For such corresponding rays the wave frequencies f_O and f_X are related by

$$f_O^2 = f_X(f_X - FH), \quad \text{or} \quad f_X = 0.5FH + (f_O^2 + 0.25FH^2)\cdot 5 \qquad (C2)$$

A change of 5% in the "apparent" value of FH corresponds to a consistent error (of about 0.03 MHz, at $f_X > 1.5FH$), in the scaled values of f_X. This error will often be a limiting factor in ionogram analysis. For valley calculations it was shown by Lobb and Titheridge (1977a) that errors of 1% in foE can prevent calculation of more than one valley parameter. The same situation applies if foE is correctly determined but following values of both f_O and f_X have a consistent error of 1%. If only one component (f_X) has this error, the situation is worse.

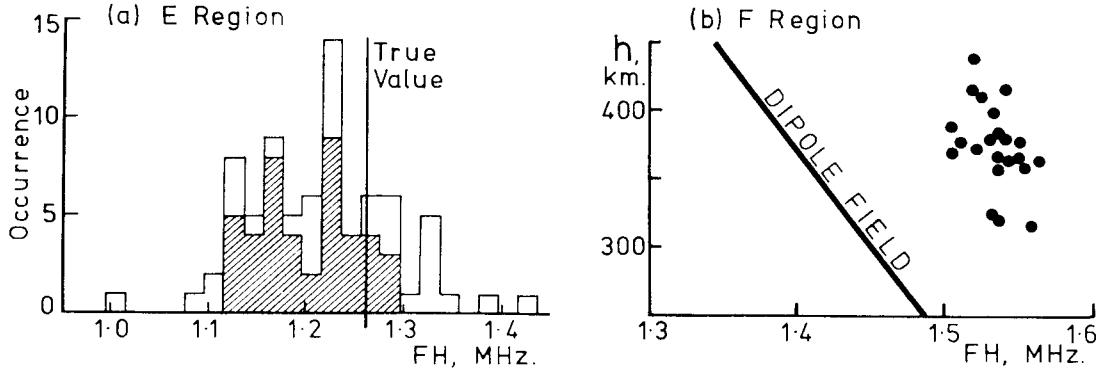

Figure C1. Values of gyrofrequency FH calculated from measurements on corresponding O and X ray cusps. Results (a) are for the E region, at a dip angle of 67° (the shaded area applies to the more accurate measurements); (b) are from F region measurements at Brisbane (Ellis, 1957).

C.2 Changes near reflection

For ordinary ray calculations at a dip angle I of 0°, results are independent of the magnetic field. At other dip angles the group retardation increases slightly with FH. A change of 5% in FH alters the virtual height, measured from the bottom of a parabolic layer, by less than 0.3% at dip angles of up to 70°; this is less than the normal experimental accuracy and has a negligible effect on real-height calculations.

For extraordinary ray calculations, changes in FH near reflection affect the virtual heights in 2 ways. These are: (i) through changes in the real height of reflection h_R, caused by changes in the plasma frequency FR required to reflect the ray; and (ii) through changes in the amount of group delay D. Thus the virtual height may be written

$$h'_X = h'(f_X) = h_R + D \qquad (C3)$$

where all terms depend on FH.

The real height of reflection h_R, for a wave of frequency f_X, is at the plasma frequency FR given by

$$FR^2 = f_X (f_X - FH) \qquad (C4)$$

If the vertical plasma-frequency gradient in the reflection region is $G = d(h_R)/d(FN)$, the dependence of reflection height on gyrofrequency is

$$d(h_R)/d(FH) = -G.f_X/2FR \qquad (C5)$$

For typical conditions at the start of a profile calculation, with $FH \simeq 1.3$ MHz and $f_X \simeq 2.1$ MHz, an error of +2% in FH gives an error of -0.021 MHz in FR. This corresponds to a decrease of about 1 km in the real height of reflection, for typical profile gradients G of 25 to 50 km/MHz in the start region (e.g. Fig. C5). Above the E/F valley, profile gradients commonly exceed 100 km/MHz. At fc = 3.5 MHz, an error of +2% in FH then gives an error of about -2 km in the real height of reflection. Real-height errors of 1 or 2 km are not very significant in themselves. They are, however, sufficient to upset start and valley calculations which depend on the difference in the group retardation of O and X rays reflected at the same real height h_R.

The group retardation for an extraordinary ray, reflected at a real height h_R, is

$$D = h'(f_X) - h_R = \int_0^{h_R} (\mu'_X - 1)\, dh \qquad (C6)$$

where μ'_X is the group refractive index at the frequency f_X. For conditions near reflection it can be shown that

$$\mu'_X T \simeq T + 0.35(1-T)(3f_X-FH)/(f_X-FH) \qquad (C7)$$

where $T^2 = 1 - (FR/f_X)^2$ and FR is the plasma frequency at reflection. The magnetic dip angle does not appear in (C7), since μ'_X is approximately independent of dip angle near T = 0.45, and the variation with dip angle is of opposite sign above and below this point. (C7) therefore gives a reasonable first-order estimate at all dip angles, for calculations which involve an integral of μ'_X up to the reflection point (T = 0).

For a constant gradient G = dh/dFN near reflection, the group delay then becomes

$$D \simeq 0.2\ G\ f_X{}^{.5}(3f_X-FH)/(f_X-FH)^{.5} \qquad (C8)$$

At a given wave frequency f_X, this leads to

$$dD/dFH \simeq 0.1\ G\ f_X{}^2(f_X+FH)/FR^3 \qquad (C9)$$

With typical values for the gradient G at reflection, this result shows that an increase of 2% in FH leads to an increase of 1 or 2 km in the group delay D. Thus changes in the terms h_R and D in equation (C3) are of similar size and of opposite sign, at all dip angles. The two effects cancel, giving $dh'/dFH \simeq 0$, for $f_X \simeq 1.5FH$.

If Δh_R and $\Delta h'_X$ are the changes in real and virtual height due to a given change in FH, (C5) and (C9) give

$$\Delta h'_X/\Delta h_R \simeq 0.75\ (1 - .5FH/(f_X - FH)) \qquad (C10)$$

Dip angle variations are quite small so (C10) provides good accuracy at medium latitudes. Over all dip angles, the maximum error in $\Delta h'_X$ is ± 0.04 km at $f_X < 2FH$, and $\pm 20\%$ at $f_X > 2FH$.

For start calculations with values of FR between about 1.0 and 1.5 MHz, FH variations produce changes in virtual height which are less than the changes in real height by a factor of 4 or more, at all dip angles. For valley calculations ($FR \simeq 2$ to 4 MHz) the changes are reduced by a factor of about 2. The need for accurate values of FH near reflection is therefore considerably eased by the opposing effects of the changes in real height and in group delay.

Some exact calculated changes in reflection height and group delay, for a linear layer and a decrease of 4% in FH, are shown in Table C1. The changes in h'_O are typically less than 0.2 km, at the low frequencies used in start calculations. The X ray results are for fixed wave frequencies f_X, corresponding to the tabulated O rays when FH = 1.2 MHz. The change Δh_R in the reflection height, due to a 4% decrease in FH, is independent of dip angle and is about +2.0 km at low frequencies. The corresponding changes in group delay are about -1.5 km, so that the decrease in FH produces an overall virtual-height increase $\Delta h'_X$ of only about 0.5 km.

Table C1 is calculated for a constant gradient dh/dFN of 50 km/MHz. This is near the upper limit for normal profiles, in the start region. Fig. C2 shows the changes in h'_X for a gradient of 20 km/MHz extending only down to FN = 0.8 MHz. Limiting the amount of low-density ionisation in this way reduces the cancellation of group-retardation and height-of-reflection changes, so that the values of $\Delta h'_X$ increase at low frequencies. For the normal range of start calculations the error of 4% in FH gives effective errors of 0.27 to 0.6 km in h'_X. The corresponding errors in h'_O are 0 to 30% as large, and of opposite sign. For combined O and X ray calculations, consistent errors $\Delta h'_O$ and $\Delta h'_X$ in the virtual heights produce a real-height error, at $FN \simeq 1.4FH$, of

$$\Delta h_R \simeq 2.8\Delta h'_O - 1.8\Delta h'_X \qquad (C11)$$

Thus a consistent error of 4% in the values of FH at reflection, corresponding to an error of 90 km in the height at which FH is evaluated, gives errors of about 0.5 to 1.5 km in real height at low frequencies.

TABLE C1. The changes (in km) in real height h_R, group delay D and virtual height h', for a reflecting layer with a constant gradient dh/dFN of 50 km/MHz, when FH decreases from 1.20 to 1.15 MHz.

	O RAY		EXTRAORDINARY RAY								
FR	$\Delta h'_O$ at		FX	Δh_R	DELAY D_X, ΔD_X, at			$\Delta h'_X$, $= \Delta h_R + \Delta D_X$		
	50°	80°			DIP= 20°	50°	80°	20°	50°	80°
1.0	-.07	-.21	1.77	2.16	77, -2.3	74, -2.2	71, -2.1	-0.13	-0.04	0.03
1.2	-.09	-.25	1.94	2.00	79, -1.8	76, -1.7	73, -1.6	0.24	0.33	0.39
1.4	-.12	-.29	2.12	1.87	83, -1.4	80, -1.4	77, -1.3	0.42	0.51	0.58
1.8	-.16	-.35	2.50	1.72	92, -1.1	90, -1.0	85, -1.0	0.60	0.70	0.77
2.2	-.20	-.40	2.88	1.62	102, -0.9	100, -0.8	95, -0.8	0.67	0.78	0.84
3.0	-.26	-.48	3.66	1.52	124, -0.8	122, -0.7	116, -0.6	0.71	0.85	0.93
4.0	-.32	-.55	4.65	1.45	153, -0.7	147, -0.6	144, -0.5	0.71	0.87	0.96

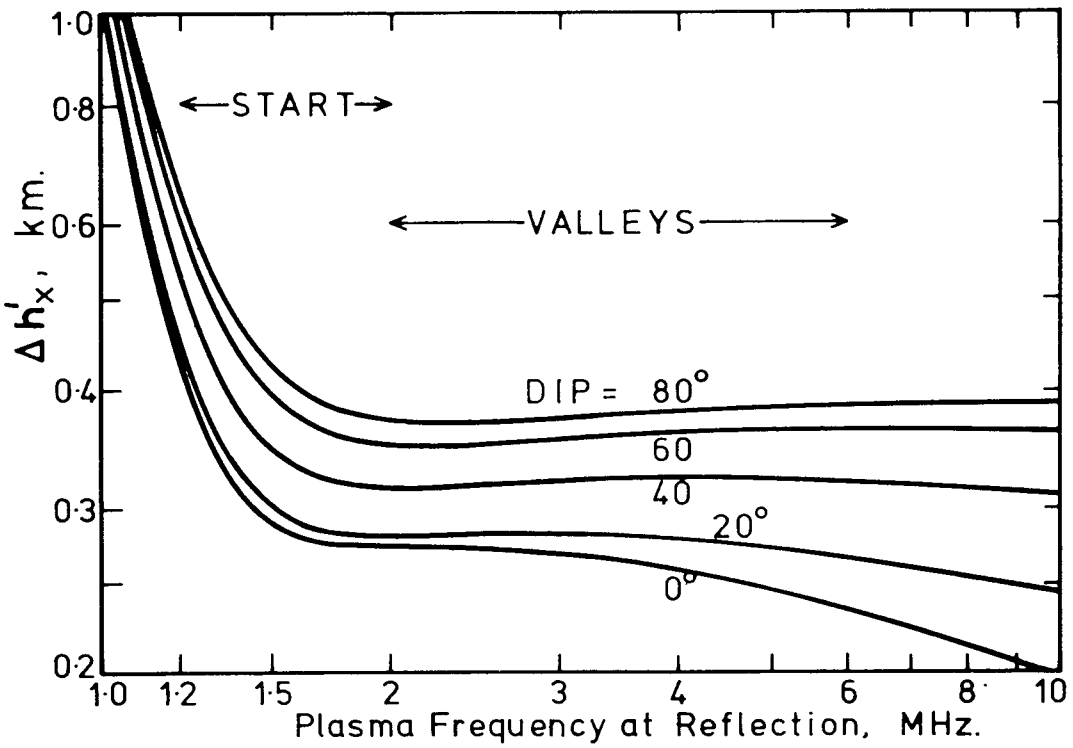

Figure C2. Changes in the X ray virtual height, at a fixed observing frequency, when the gyrofrequency FH is decreased from 1.20 to 1.15 MHz. Calculations are for a reflecting region with dh/dFN = 20 km/MHz at FN > 0.8 MHz, and no ionisation at FN < 0.8 MHz.

C.3 Retardation in the underlying region

For dip angles I greater than about 10°, and plasma frequencies FN much less than the wave frequency F, refractive indices in the ionosphere are close to the quasi-longitudinal approximation. Neglecting terms in $(FN/F)^4$, the group refractive index μ' becomes

$$\mu' \simeq 1 + .5\ FN^2 / (F \pm FH \sin I)^2 \qquad (C12)$$

where upper and lower signs refer to the O and X rays respectively. Thus the group retardation due to low-density ionisation is

$$D = \int (\mu'-1)\ dh \simeq .5(F \pm FH \sin I)^{-2} \int FN^2\ dh \qquad (C13)$$

The integral is proportional to the total electron content of the underlying ionisation. For "corresponding" O and X ray frequencies F and FX (reflecting at the same plasma frequency FR), (C12) gives the ratio of the group retardations as

$$R_{X,O} = D_X/D_O = ((FR + FH \sin I)/(FX - FH \sin I))^2 \qquad (C14)$$

The change ΔD in the group retardation, due to a change ΔFH in the gyrofrequency, is obtained from (C13) as

$$\Delta D/D = \mp\ 2\Delta FH \sin I\ /\ (F \pm FH \sin I) \qquad (C15)$$

Values of $R_{X,O}$ from (C14) are shown in Table C2. For dip angles above 30°, and FR < 2FH (as in most starting calculations), the group delays are typically 4 times larger for the X ray. From (C15) we see that the percent variations in the delay, due to changes in FH, are about twice as large for the X ray as for the O ray.

The results of Table C2, and equations (C12) to (C15), are accurate for low-density ionisation. Results for higher densities are shown in Table C3, calculated for FN increasing linearly from 0.4 to 0.8 MHz. The O-ray delays D_O are approximately independent of FH, but vary considerably with dip angle. X-ray delays D_X are less dependent on the dip angle and highly dependent on FH. For FR = 1.2FH to 2.2FH (the common range for start calculations), group delays are typically about 4 times larger for the X ray than for the O ray. Changes in FH alter the group delay by an amount ΔD which is 10 to 100 times larger for the X ray. Thus to determine the errors which result from an incorrect FH, in the underlying regions, we need consider only the changes in delay for the X ray.

The amount of low-density ionisation used for the calculations in Table C3 is quite typical for night-time profiles. The two mean Arecibo profiles are shown in Fig. C5(a). Approximating the low-density ionisation by a linear increase from 0.4 to 0.8 MHz gives a thickness for this section of about 60 km for model 3A, and 160 km for model 3B. An independent set of mean night-time curves is shown in Fig. C5(c) (from Knight, 1972). Approximating the underlying ionisation in these profiles by a linear increase, from 0.4 to 0.8 MHz, requires a thickness of about 100, 80 and 60 km at 1, 2 and 6 hours after sunset. Thus real-life profiles commonly have delays similar to those in Table C3; and an error of 4% in the assumed value of FH for the underlying region alters h'_X by (typically) 1 to 5 km, at the frequencies used in start calculations.

Errors in the value of FH used for underlying regions of ionisation are unavoidable. The continuous lines in Fig. C3 represent a simplified model for the night-time ionosphere. This has a parabolic E layer extending from 100 to 180 km (corresponding roughly to the mean variation in Fig. C5(a)), and a sharply-bounded reflecting region at 220 km. Virtual heights for the O and X rays are shown by the solid lines in Fig. C4. These were calculated using an inverse-cube variation of FH, for typical ground values FB at each dip angle. Analysis of the virtual heights can give, at best, the equivalent monotonic profile shown by the broken line in Fig. C3. This has the same total electron content as the original profile, as required for accurate calculations of F layer heights at high frequencies. At the low frequencies used in start calculations, however, the smaller values of FH at the height of the equivalent monotonic profile cause an appreciable increase in the virtual heights of

Table C2. The relative group retardation $R_{X,O}$ giving the ratio of group delays for "corresponding" X and O rays (reflected at the same plasma frequency FR) for low-density regions of the ionosphere where FN << FR.

FR/FH	FX/FH	DIP = 0	20	30	40	50	60	70	80	90 deg
1.0	1.62	1.00	1.10	1.80	2.84	4.30	6.16	8.18	9.82	10.47
1.4	1.99	1.00	1.12	1.63	2.31	3.15	4.09	4.99	5.67	5.92
2.0	2.56	1.00	1.11	1.47	1.90	2.37	2.86	3.29	3.58	3.69
4.0	4.53	1.00	1.07	1.25	1.43	1.60	1.76	1.89	1.98	2.00

Table C3. Group delays D (in km) for an underlying region in which FN increases linearly, from 0.4 to 0.8 MHz, in a height range of 100 km. D_O and D_X are for "corresponding" frequencies FR and FX at FH = 1.20 MHz. ΔD_O and ΔD_X are the changes which occur when FH is increased to 1.25 MHz (with no change in FX).

O-RAY:	D_O, ΔD_O at DIP =			X-RAY:	D_X, ΔD_X at DIP =		
FR	20°	50°	80°	FX	20°	50°	80°
1.0	28.2, .01	18.1, .07	5.8, -.22	1.72	64.4, 19.6	75.3, 20.6	81.9, 20.8
1.2	16.0, .01	9.1, -.04	4.2, -.16	1.90	29.3, 5.23	36.6, 6.17	41.4, 6.75
1.4	10.6, .00	6.0, -.05	3.4, -.12	2.09	16.9, 2.12	21.8, 2.67	25.0, 3.05
1.7	6.6, .00	3.9, -.04	2.6, -.08	2.37	9.3, .78	12.1, 1.04	14.0, 1.33
2.0	4.5, .00	2.9, -.04	2.1, -.06	2.65	6.0, .37	7.7, .51	8.9, .61
2.4	3.1, .00	2.1, -.03	1.6, -.04	3.04	3.8, .17	4.8, .24	5.5, .30
3.0	1.9, .00	1.4, -.02	1.1, -.03	3.63	2.2, .06	2.8, .10	3.1, .13
4.0	1.1, -.01	0.8, -.01	0.7, -.01	4.61	1.2, .02	1.4, .03	1.6, .05

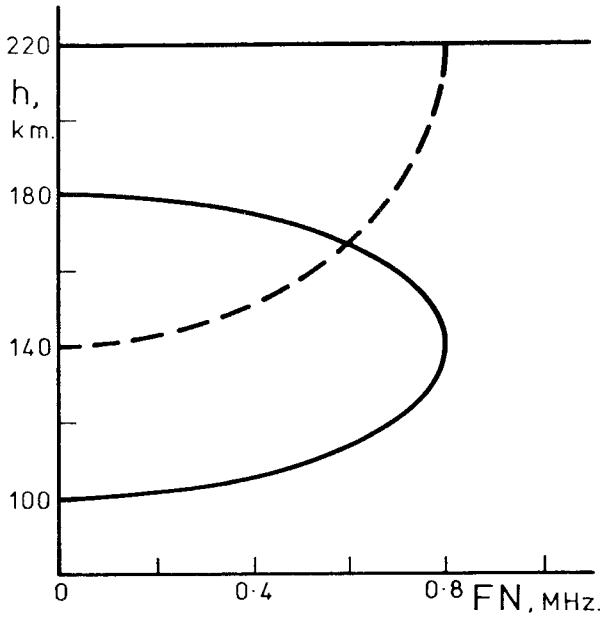

Figure C3. A simple parabolic model for the night-time E layer (solid line), and the equivalent monotonic distribution (broken line) for an F layer with a sharp lower boundary at 220 km.

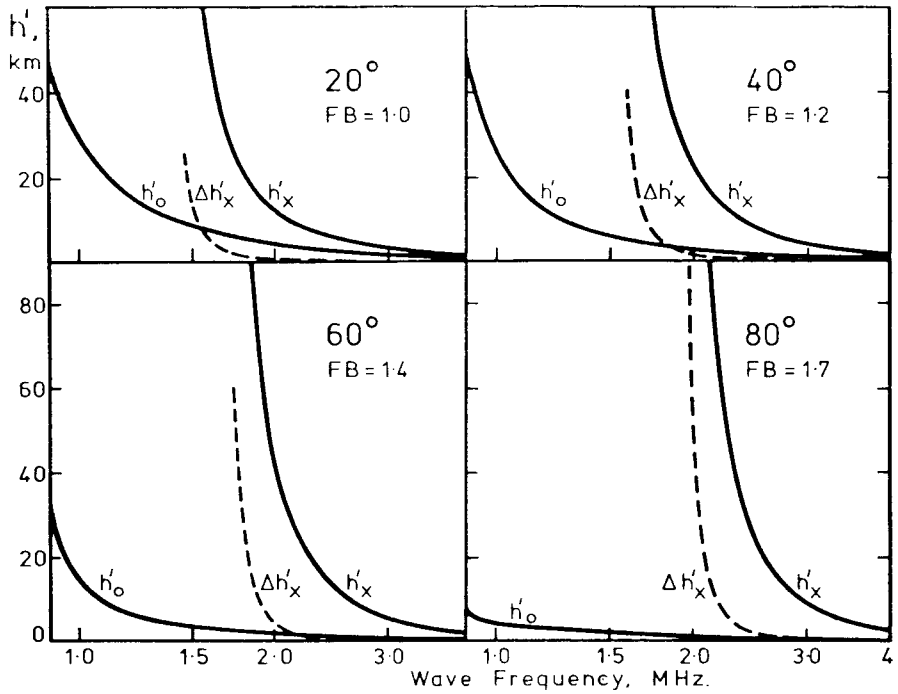

Figure C4. Solid lines show the virtual heights for the O and X rays, calculated from the model of Fig. C3, at 4 different dip angles. FH has an inverse-cube variation with height, from the indicated ground values FB. Broken lines show the change in h'_X when the true profile is replaced by its equivalent monotonic distribution.

the X ray. This increase $\Delta h'_X$, plotted as a broken line in Fig. C4, represents an effective error in the values of h'_X. The $\Delta h'_X$ curves, like the values of h'_O, begin at the wave frequency for which FN = 0.9 MHz at reflection. At this frequency the effective error (in km) of the X ray virtual heights is roughly equal to the dip angle in degrees. For FN = 1.0 MHz at reflection, the effective error is roughly one third of the dip angle, or 10% of $(h'_X - h)$. These errors are caused by the increase of about 60 km in the mean height of the underlying inisation, and the corresponding decrease in FH, when we replace the true variation in Fig. C3 by its monotonic equivalent.

C.4 Model studies

Profiles 3A,3B and 8A,8B,8C,8D in Figure C5 were developed within URSI Subgroup G/6/2 to test ionogram analysis procedures. For each profile accurate virtual heights were calculated, at dip angles of 30° and 70°, using an inverse-cube variation of FH with height. The results were analysed by different procedures assuming values of fmin (for both the O and X components) corresponding approximately to plasma frequencies of 0.8 and 1.5 MHz at reflection.

The program POLAN uses iteration to determine the correct FH at reflection for each data frequency. This is to ensure a correct plasma frequency at reflection for the X rays, so that the relative reflection heights of O and X ray data would be correct. At the time of the URSI tests (1976-77) this was considered the prime requirement for accurate results. The study of Section C.2 has since shown that errors due to an incorrect FH at reflection are considerably reduced by the opposing effects of group delay and reflection height variations.

The relative importance of a correct FH at reflection, and a correct FH for the underlying ionisation, is shown in Table C4. (a) gives the errors in the calculated real heights at 1.5 MHz, as originally obtained from the series of URSI tests (Gulyaeva et al, 1978; McNamara, 1978b) using the value of FH at reflection for each ray. Four sets of data were analysed for each model, corresponding to the two dip angles and two starting frequencies noted above. Table C4(b) gives results from the same input data but assuming a constant gyrofrequency, corresponding to a height of 170 km, throughout the calculation. These results are obtained from a single least-squares solution, with no iteration. The height of 170 km is chosen as representing an approximate mean centre for the underlying ionisation regions.

The physical constraints discussed in Section 8.7 were not employed in the tests of Table C4. The overall improvement by a factor of 3.2 in the (mean + RMS) errors, from (a) to (b), is therefore due entirely to the different values of FH. The large maximum errors in the 3A,B data set are due to the "difficult" profile 3B which, as discussed in section 8.5.2, would not normally be analysed from low values of fmin. The overall conclusion from these calculations is clear: at both high and low dip angles, and with all tested profiles, a correct FH for the unseen regions is far more important than a correct FH at reflection.

Table C4. Errors in the calculated real heights at a plasma frequency FN = 1.5 MHz, using the 'slab start' in POLAN to analyse virtual-height data corresponding to the profiles of Fig. C5. For each data frequency the same value of FH is used throughout the ray path. Results (a) are for FH equal to the value at the reflection height of each ray, while (b) uses a constant FH corrresponding to a height of 170 km.

Profiles Analysed:		3A, 3B (8 data sets)			8A,B,C,D (16 data sets)			
ERRORS AT 1.5 MHz:		MEAN	RMS	MAX	MEAN	RMS	MAX	
(a) Using FH at reflection.								
POLAN MODE =	4	2.8	3.6	7.6	1.29	1.41	2.3	km
	5	2.2	2.9	4.8	1.26	1.47	2.4	km
	6	1.8	2.5	4.8	1.11	1.31	2.4	km
(b) Using FH at 170 km.								
POLAN MODE =	4	0.50	0.77	4.4	0.47	0.61	1.3	km
	5	0.72	1.04	2.3	0.42	0.55	1.1	km
	6	0.57	0.76	1.6	0.43	0.64	1.9	km

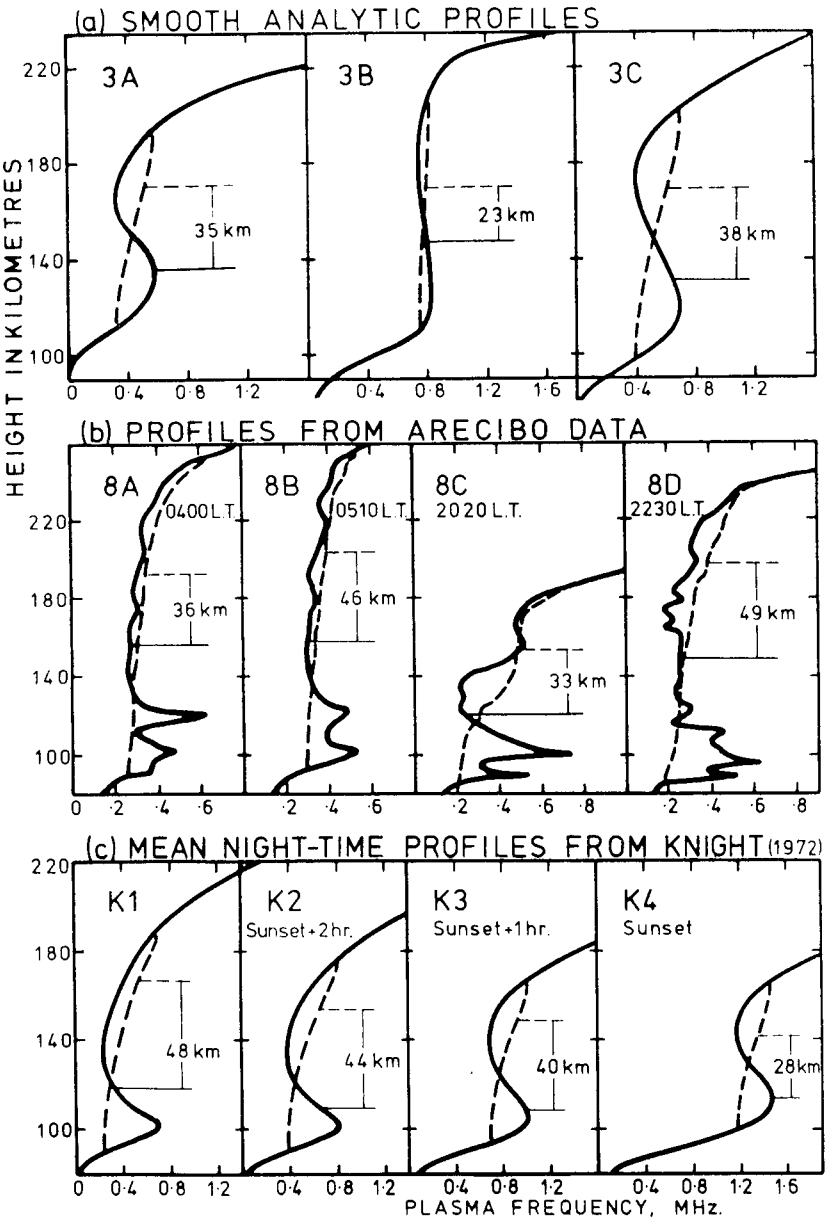

Figure C5. Night E-region profiles used in developing rules for start calculations. Solid curves show the actual profiles, while broken lines are the equivalent monotonic distribution. Horizontal lines indicate the weighted mean heights for gyrofrequency calculations, for both the solid and broken line profiles.

3A and 3B are smoothed analytic approximations to the two main types of Arecibo profile observed during the magnetically quiet night of 12 April 1972 (Brice, private communication). 3C is a similar type of curve produced as the sum of two overlapping Chapman layers (Appendix H.2). The reflecting F region in 3C is almost identical in shape to models K1 and K2, while the underlying variations approximate an average of the extreme mean types K1, K2 and 3B.

8A to 8D give individual profiles obtained by the Arecibo backscatter facility. The early morning profiles 8A,8B were obtained on 26 July 1972, and the evening profiles 8C,8D on 11 April 1972. Curves shown are smoothed versions of the data from McNamara and Titheridge (1977).

K1 to K4 are idealised variations derived by Knight (1972) from a synthesis of 97 published profiles based on rocket, backscatter, ionogram, partial reflection, full-wave integration and cross-modulation measurements. K1 applies from 6 hr after sunset to 2 hr before sunrise.

C.5 The choice of gyrofrequency for the underlying regions

Different models which have been used for the lower night ionosphere during the present study are summarised in Fig. C5. Solid lines show the actual profiles, while broken lines are the equivalent monotonic distributions. The monotonic profile maintains the same total amount of ionisation, in any range of FN, but the ionisation is effectively moved upwards to regions of lower gyrofrequency. The original position of this ionisation, and hence the correct value of FH to use in calculating the delay it produced, cannot be found from analysis of the ionograms.

Horizontal solid lines in Fig. C5 indicate the approximate mean height at which the gyrofrequency FH must be determined, if a fixed value of FH is to give the correct overall retardation for the true (solid line) profiles. The horizontal broken lines give mean gyrofrequency heights appropriate to the equivalent monotonic distribution. The two heights differ by 23 to 49 km, with a mean difference of 38 km.

Ionogram analysis provides only a simplified two-parameter representation of the underlying ionisation (Section 8.1). This can differ considerably from the true equivalent-monotonic profile. Thus for calculating the group retardation in the underlying region, a mean gyrofrequency height determined from the calculated profile is typically too high by 50 km. In some cases, such as those illustrated in Figs. 12 and 13 of Section 8.4, the mean gyrofrequency height derived from the ionogram is 100 km too high.

The value of gyrofrequency FH to use in start calculations, for calculating the group delay in the underlying ionisation, is therefore best determined from a model. The simplest model would use a fixed height for night-time calculations. A value of 140 km is accurate to within about 30 km under most conditions. For the 11 profiles of Fig. C5, the mean gyrofrequency height for the true (solid line) profiles ranges from 109 to 158 km with a mean value of 131 km.

Errors in the mean gyrofrequency height (FHHT) can be further reduced with a time-varying model. Fig. C5 suggests FHHT increasing from about 120 km near sunset (profiles 8C and K2 to K4) to 150 km later in the night (8A,B,D, and K1; the mean heights shown are for FN less than about 0.9 MHz, and will increase appreciably in model K1 for higher values of fmin). This variation follows approximately the night-time "starting height" h_s, which is used for beginning an analysis in the absence of X ray data (Section 6.4). h_s is normally provided as the parameter START in POLAN. If START = 0, h_s is taken as the least of (i) a value estimated by extrapolation of the absolute virtual-height gradient to zero frequency, and (ii) the value $h_s = 0.3h'min + 80$ km.

The second condition limits h_s to 140 km at h'min = 200, and 160 km at h'min = 270 km. A simple and approximately optimum value of FH for use in X ray starting calculations is therefore obtained by setting FHHT equal to the starting height h_s which would be used in the absence of X rays.

C.6 The separation of underlying and reflection regions

Early versions of POLAN used a fixed value of FH, corresponding to the starting height FHHT described above, only for the linear slab section of the start profile. The polynomial section (at FN > 0.6fmin) used the value of FH at the calculated reflection height for each ray, to ensure that corresponding O and X rays were reflected at the same true height. For most profiles the height changes are not large in the polynomial section, and this procedure gives good results. It fails badly however, when a large part of the underlying ionisation has FN > 0.6fmin. The calculated polynomial then extends down to low heights, and includes much of the low level ionisation, so that use of the value of FH at reflection gives appreciable errors in the calculation of group retardation.

Test profiles 3A and 3B are shown by the heavy lines in Fig. C6. Using a constant value of FH, virtual heights were calculated for these profiles at a frequency interval of 0.1 MHz. Analysis by POLAN from fmin = 1.0 MHz gives the real heights shown by the solid dots in Fig. C6. Thin lines show the approximate representation obtained in the unobserved regions, at FN < 1.0 MHz. This consists of a linear-in-FN step from a to b, and a polynomial section at higher frequencies (with FN > 0.6fmin). For model 3A the result represents adequately the amount of low-density ionisation. For model 3B the underlying ionisation has a mean plasma frequency greater than 0.6fmin. The POLAN result simulates this by a polynomial section which drops rapidly, through more than 250 km, below 0.8 MHz; plus a negative slab section denoting a negative amount of ionisation at FN < 0.6 MHz. This unphysical distribution gives, mathematically, approximately the correct values for the integrals of FN^2 and FN^8 in the unseen region (Appendix G.2). The calculated real heights are accurate to within 0.3 km at f > 1.1 MHz. POLAN will normally require that the thickness of the linear slab be positive or zero, unless this condition significantly worsens the fit to the virtual-height data. Calculated real heights are then as shown by the broken lines in Fig. C6, and are accurate to within 0.7 km at f > 1.1 MHz.

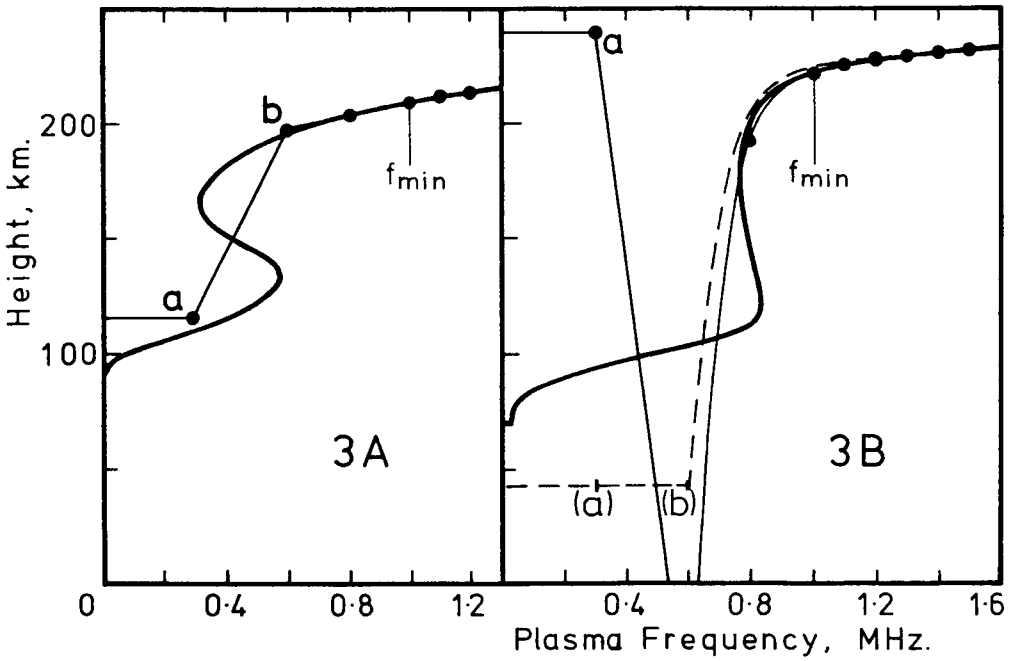

Figure C6. Starting calculations using a fixed gyrofrequency FH = 1.2 MHz, at a dip angle of 70°. Heavy lines give the original model profiles, while solid dots are the result of starting calculations with fmin = 1.0 MHz. The broken line for model 3B is the solution obtained if the thickness of the underlying slab a,b is constrained to be zero instead of negative.

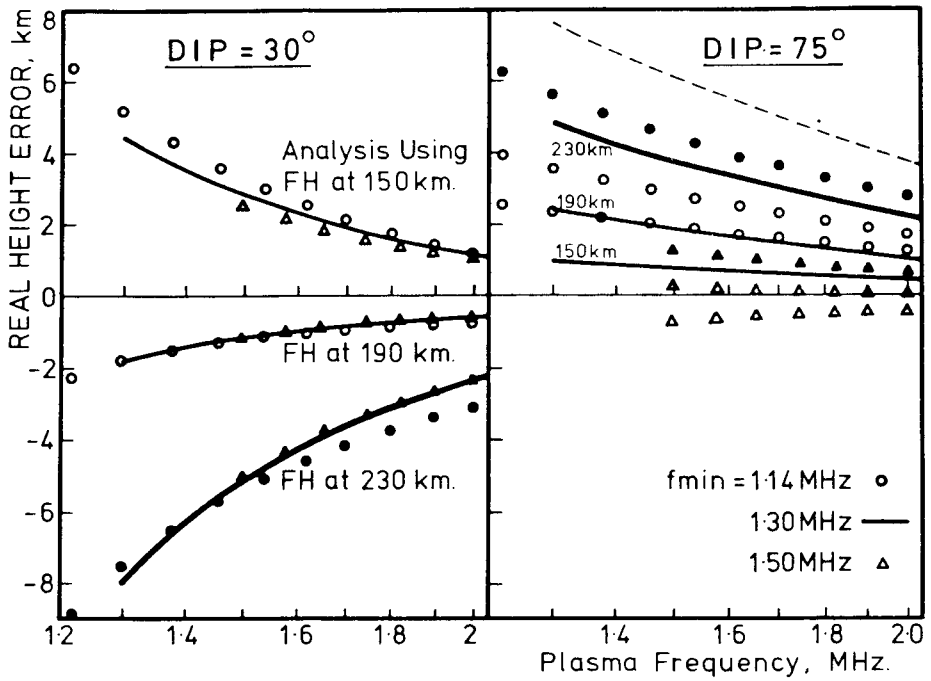

Figure C7. Variable FH data corresponding to the model 3B (Fig. C6) analysed using fixed values of FH corresponding to heights of 150, 190 and 230 km. For each value of FH, the circles, lines and triangles use data corresponding to plasma frequencies of 1.14 (.08) 1.54; 1.3 (0.1) 1.7; and 1.5 (0.1) 1.9 MHz respectively. Solid symbols, and heavy lines, are for the smallest value of FH (at 230 km).

Ionograms calculated for the profiles of Fig C6, with a height-varying gyrofrequency, were used for Test 6 of URSI WG G/6/2 (McNamara 1978b). Fig. C7 shows the errors resulting from analysis of the 3B data under different conditions and assuming a constant value of FH. At dip 30° results vary only slightly with the value of fmin (since at this dip angle real heights can, in fact, be found independently of the underlying ionisation; Section 8.1 and Titheridge, 1974b). Calculated heights decrease as FH increases, and are approximately correct for FH corresponding to a height FHHT of about 180 km. This is close to the mean height for the underlying and reflection regions. Reflection heights are about 230 km for model 3B, so the bottom curve in Fig. C7 corresponds to the use of FH at reflection. This gives large negative errors at dip 30°.

At dip 75°, calculated heights increase as FH decreases. (Note that the sensitivity of the results to changes in FH does not pass through zero between dips 30° and 75°, but becomes large and unstable in a narrow range of dip angles from 33 to 38°; this is the ill-defined region discussed in Appendix B.2 at which practical O/X calculations become impossible.) Results now depend on the representation of the unseen ionisation, and vary with fmin. The upper continuous line in Fig. C7 is for a fixed FH corresponding to a height of 230 km; this gives quite closely the errors which occur if the value of FH at reflection is used throughout the path of each ray. The broken line is the error obtained if, in addition, the underlying ionisation is forced into a physically acceptable shape. This broken line closely reproduces the extreme errors obtained for this model in the URSI tests. (In normal work, as noted in Section 8.4, the physical constraints are not enforced when they significantly increase the virtual-height fitting error).

To avoid these errors we must use a value of FH corresponding to some height below the reflection point, if the polynomial real-height section includes a large amount of the underlying ionisation. This case is typified by the model 3B profile. Calculated results from fixed-FH data are shown in Fig. C8. Using fmin = 1.5 MHz (the profile b,b',b",B) we get the normal result in which most or all underlying ionisation is represented by the linear slab section b,b'. At fmin = 1.0 MHz the polynomial section begins at a' where h = -72 km and dh/dFN = 2900 km/MHz. It represents primarily the underlying ionisation up to the point a", at 0.8 MHz, and follows the true profile reasonably well at higher frequencies. The boundary between underlying and reflection regions therefore occurs near a".

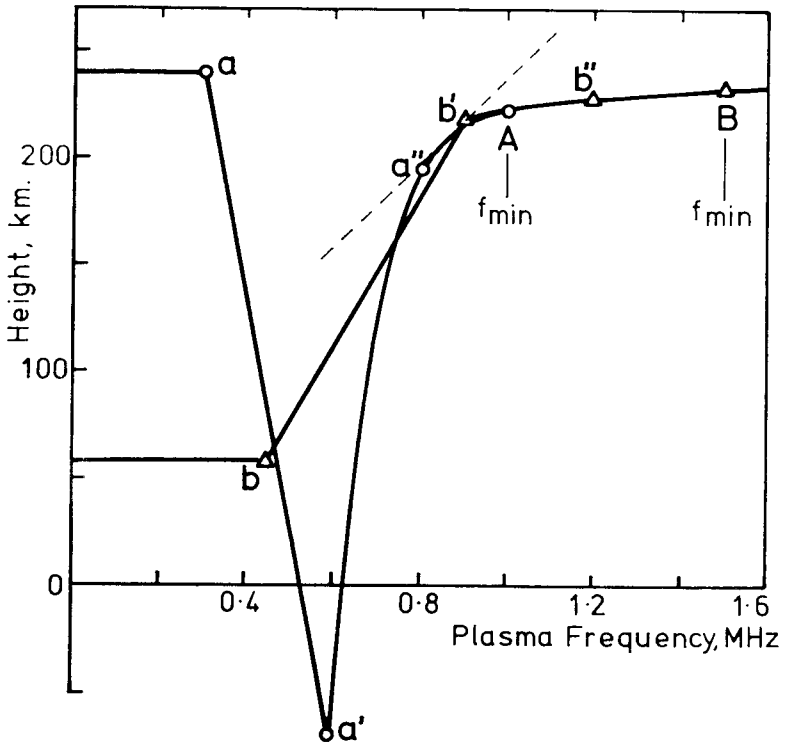

Figure C8. Calculated profiles from fixed-gyrofrequency data for model 3A. Points a to A correspond to an analysis with fmin = 1.0 MHz, the lower case letters denoting additional calculated points below fmin. b to B are for fmin = 1.5 MHz. The broken line corresponds to a gradient dh/dFN of 200 km/MHz.

The transition from underlying to reflecting region is defined most effectively by the change in gradient. Studies under different conditions suggest placing the boundary where the profile gradient is about 200 km/MHz, corresponding to the broken line in Fig. C8. This appears reasonable for most "difficult" profiles, and also defines the correct point b' (Fig C8) or b (Fig C6) for normal calculations where the initial gradient of the polynomial is less than 200. To include some additional cases where gradients can be less than 200 km/MHz over part of the underlying region, the following rules are used.

(1) A profile is NORMAL if (a) the thickness of the linear slab section is positive, and
(b) the initial gradient of the polynomial section is less than 200 km/MHz.
If either (a) or (b) is false, the profile is considered DIFFICULT.

(2) For NORMAL profiles, the model height FHHT of Section C.4 is used to define FH for the linear slab section. The calculated height at the first scaled X-ray frequency above fmin is used to determine FH for the entire reflection region (beginning at b' in Fig. C8). This ensures the correct relative retardation at different frequencies, if the polynomial does curl down appreciably at lower frequencies, and is allowable because of the insensitivity of the results to small errors in FH at the individual reflection points (Section C.2).

(3) A DIFFICULT profile has appreciable retardation from underlying ionisation with FN > 0.7fmin. The initial section of the polynomial then represents underlying ionisation, and integration through this section should use the gyrofrequency appropriate to the height FHHT. If the calculated gradient at FN = 0.8fmin (the point a" in Fig. C8) is less than 200 km/MHz, the reflection region is assumed to begin at this point. Otherwise the gradient G is calculated at FN = 0.9fmin. If this value is less than 200 km/MHz, the frequency (between 0.8fmin and 0.9fmin) corresponding to G = 200 is determined by linear interpolation. If G exceeds 200 at 0.9fmin, then this frequency (0.9fmin) is taken as the boundary between underlying and reflection regions.

The reflection integral for difficult profiles starts from some frequency in the range 0.8fmin to 0.9fmin. The upper limit is set to enable a reasonable calculation of the group retardation near reflection, for the lowest scaled frequency fmin. A lower limit of 0.8fmin is used to cope with cases where the polynomial descends through an appreciable distance, at frequencies of about 0.7 to 0.8fmin, with a gradient just less than the allowable limit of 200 km/MHz. Thus with a negative slab thickness, or with G > 200 km/MHz at 0.6fmin, an initial range of at least 0.2fmin of the polynomial section is allocated to base ionisation. If in fact there is little base ionisation, so that the mean gradient in the range 0.6 to 0.8fmin is less than 200 km/MHz, then the height interval covered by this range of frequencies is reasonably small (less than 50 km, at FN < 1.2 MHz) and using the "underlying" gyrofrequency does little harm. Separation of the polynomial integrals into two parts, using different values of FH, is carried out within the subroutine COEFIC as described in Appendix D.1